CONDITIONS FOR SPATIAL INSTABILITIES AND PATTERN FORMATION FROM MONOMIAL STEADY STATE PARAMETERIZATIONS

CARSTEN CONRADI, MAYA MINCHEVA, AND HANNES UECKER

Abstract. We study the onset of spatial instabilities in reaction networks where the spatially homogeneous system admits a steady state parameterizations. We formulate a sufficient condition – based on the signs of the constant and leading coefficients of the characteristic polynomial of the linearized Jacobian scaled by the diffusion coefficients – that guarantees a Turing-like instability to spatially inhomogeneous solutions on appropriately chosen domains Ω. We also present a specific condition on the domain size $|\Omega|$ required to trigger this instability. As a consequence of employing a monomial parameterizations, these conditions take the form of algebraic polynomial inequalities involving only rate constants and diffusion coefficients. We apply these ideas to a network describing the sequential and distributive (de-)phosphorylation of a protein at two binding sites, ultimately deriving a condition involving only the four catalytic constants of the enzymes and the diffusion coefficients of the four enzyme-substrate complexes that guarantees a Turing-like instability.

Contents

1. Introduction

The emergence of spatial patterns in biochemical networks is an active area of research, see e.g. [20, 24]. A seminal mechanism for pattern formation in reaction–diffusion systems has been introduced by Alan Turing in [34] (c.f. for example, [21] and the contributions [1, 19] on the occasion of the 70th anniversary of the paper). The mechanism consists of a reaction system of two interacting chemicals. Two scenarios are considered: (i) the homogeneous, well mixed case when diffusion is negligible and the dynamics of the species can be described by a pair of ODEs; and (ii), the inhomogeneous case when diffusion cannot be neglected and the dynamics is described by a pair of reaction-diffusion PDEs. In scenario (i) the steady state of this ODE system is 'stable' (i.e. all eigenvalues of its linearization have a negative real part). In scenario (ii) this steady state corresponds

Date: April 24, 2026.

to a homogeneous, time-constant solution (a homogeneous steady state) of the PDE. In Turing's example the diffusion coefficients are chosen in such a way that this homogeneous steady state of the PDE is unstable (i.e. at least one eigenvalue of its linearization is positive) and a non-homogeneous time-constant solution emerges nearby. In this setting the non-homogeneous steady state represents a pattern that emerges when the homogeneous steady state is de-stabilized by diffusion.

Given a reaction system with fixed rate constants yielding a stable steady state of the ODE system, this 'de-stabilizing' only happens for selected values of the diffusion coefficients. Finding such values for the diffusion coefficients is straightforward in the two species case, see e.g. [17, 18, 26], but can be challenging if the number of species increases. For an arbitrary number of species only a limited number of results exists, for example, [32, 33], and, [36, 37]. In [33] a necessary and a sufficient condition for a Turing Instability are given in terms of the signs of the principal minors of the Jacobian of the ODE system. Every principal minor corresponds to what the authors call a subsystem and if the minor is of a certain sign, then the subsystem is called 'unstable'. The approach presented in [36] further extends the idea of unstable (sub-)systems: given a subsystem of size p, the authors show that by suitably choosing the diffusion coefficients and the domain one can force p eigenvalues of the linearization to approach the eigenvalues of the subsystem while the remaining eigenvalues of the linearization approach $-\infty$. And [37] allows for cross-diffusion and exploits these ideas to designing diffusion coefficients that enable instabilities.

Here we consider reaction networks that admit a monomial parametrization with any number of species, their ODEs and the corresponding reaction-diffusion PDEs on spatial domains of dimension 1, 2 and 3. Networks that admit a monomial parametrization are a generalization of the networks described in [29] and have been introduced in [6]. They form a special class of reaction networks, where all positive steady states can be parameterized. We first focus on the existence of at least one positive real eigenvalue of the linearization of the reaction-diffusion PDE. To this end we analyze a polynomial representation of the determinant of the linearization and formulate inequality conditions on the sign of its leading and constant coefficient (inequalities (3.5a) & (3.5b)). Given a monomial parametrization of all positive steady states, these inequalities represent polynomial conditions that are sufficient for the linearization to have at least one positive eigenvalue. Based on this inequality condition we formulate conditions on the domain (in 1-, 2- and 3-D) that are sufficient for the existence of such positive eigenvalues (Theorem 3.4). If the rate constants have been chosen in such a way that the steady state of the ODE is stable, then an instability occurs (Corollary 3.6). We call the corresponding instability *Turing-like* for the following reason: Usually the term *Turing instability* refers to instabilities with respect to patterns with wavelengths independent of the (asymptotically large) domain size. We, however, present conditions guaranteeing that instabilities will always arise for the lowest eigenvalues of the scalar Neumann Laplacian on Ω. Due to this reduction we do not consider all types of instabilities, but *long wave* (aka *sideband*) types: the first instability is always with respect to nonhomogeneous solutions of maximal wavelength allowed by the domain (cf. Remark 4.3 and §4 for illustration by dispersion relations).

Our approach is closely related to that of [33]: Both are based on the fact that the determinant of a matrix equals the product of all its eigenvalues and that consequently a change of the sign of the determinant indicates an odd number of real eigenvalues crossing the imaginary axis. The authors of [33] exploit the fact that the determinant of the linearization can be expressed in terms of sums of products of principal minors of the Jacobian of the ODE system (weighted by products of diffusion coefficients) and that stable and unstable subsystems lead to terms with opposite signs. Hence the existence of at least one unstable subsystem allows the determinant to change sign.

We, on the other hand, analytically compute the determinant of the linearization evaluated at all homogeneous solutions (with the help of the monomial parametrization). This yields a polynomial that has coefficients that are rational in the rate constants and diffusion coefficients. Our inequalities (3.5a) & (3.5b) then guarantee that this polynomial changes sign (at least once).

As an application we consider the network from [7]. It describes the double (de)phosphorylation of a protein S by a kinase K and a phosphatase F according to the following mechanism (S_0, S_1 and

S_2 refer to un-, mono-, and double-phosphorylated substrate):

$$\begin{aligned} S_0 + K \underset{k_2}{\overset{k_1}{\rightleftharpoons}} S_0K \xrightarrow{k_3} S_1 + K \underset{k_5}{\overset{k_4}{\rightleftharpoons}} S_1K \xrightarrow{k_6} S_2 + K, \\ S_2 + F \underset{k_8}{\overset{k_7}{\rightleftharpoons}} S_2F \xrightarrow{k_9} S_1 + F \underset{k_{11}}{\overset{k_{10}}{\rightleftharpoons}} S_1F \xrightarrow{k_{12}} S_0 + F \ . \end{aligned} \tag{1.1}$$

Here $k_1, \ldots, k_{12}$ denote the reaction rate constants. There are nine species, cf. (2.1) and three conserved quantities: the total amount of kinase, phosphatase and substrate. A reaction-diffusion PDE derived from this network additionally requires nine diffusion coefficients. Our analysis shows that the catalytic constants of the kinase with substrates S_0 (k_3), and S_1 (k_6) as well as those of the phosphatase with substrates S_2 (k_9), and S_1 (k_{12}) together with the diffusion coefficients of the enzyme substrate complexes S_0K (d_3), S_1K (d_5), S_2F (d_8) and S_1F (d_9) enable spatial instabilities in the following sense: as a consequence of Theorem 3.4 and Corollary 3.6 we show here that if the catalytic constants and the diffusion coefficients d_3, d_5, d_8 and d_9 are such that

$$\frac{k_3\, k_9}{k_6\, k_{12}} < \frac{d_3 d_8}{d_5 d_9}, \tag{1.2}$$

then the linearization of the reaction diffusion PDEs derived from network (1.1) has at least one positive real eigenvalue – for an appropriately chosen spatial domain. And if the corresponding steady state of the ODEs derived from network (1.1) is stable, then a Touring-like instability occurs. To illustrate our results we choose parameter values satisfying (1.2) and proceed with a detailed numerical analysis on a 1D- and a 2D-domain; the k_i- and d_i-values are given in Section 3.3. On both domains we find several non-homogeneous solutions and examine their local stability by numerical simulations.

The problem of genuine Turing instabilities for (1.1) remains open, as our conditions will always lead to instabilities for the lowest eigenvalues of the Neumann Laplacian. Moreover, our analysis is based on matrix determinants, i.e., on the products of eigenvalues, and hence ignores instabilities due to complex conjugate pairs of eigenvalues crossing the imaginary axis. Hence, we cannot detect pairs of complex-conjugate eigenvalues crossing. Interestingly, when examining the system (1.1) numerically, we found Hopf bifurcations nonetheless. This finding is interesting in its own right, in particular as the existence of Hopf bifurcations in the ODE model of the system (1.1) is still an open question [4, 11]. Such Hopf instabilities and associated bifurcations of time–periodic solutions do play a role in certain parameter regimes for the system (1.1) (c.f. §4, where we investigate standing wave solutions arising in a Hopf-bifurcation). Thus, while our analysis is helpful to identify some sufficient conditions for instabilities, which are also useful as guidance for the numerics in §4, it is only a first step towards a more complete picture of pattern formation in the system (1.1).

The paper is organized as follows: in § 2 we introduce the notation, the dynamical systems defined by mass action networks (ODEs and reaction-diffusion PDEs) and mass action networks that admit a monomial parametrization. In §3 we derive conditions for the occurrence of spatial instabilities, in §4 we apply our results to network (1.1), and in Section 5 we briefly summarize our results.

2. The mass action network

See for example [10] for an in-depth introduction to chemical reaction networks with mass action kinetics. We use c to denote concentrations of chemical species, Γ to denote the stoichiometric matrix defined by the network, and $r(k, c)$ to denote the reaction rates. Assuming n chemical species and r reactions, Γ is a $n \times r$ matrix, $\Gamma \in \mathbb{R}^{n\times r}$. The reaction rates are given by a function $r : \mathbb{R}^r \times \mathbb{R}^n \to \mathbb{R}^r$ that depends on the (positive) rate constant vector $k \in \mathbb{R}^r$ and the concentrations. For mass action networks it is a vector valued function with monomial entries.

For (1.1), we use

$$c_1 = [S_0], \qquad c_2 = [K], \qquad c_3 = [S_0\, K],$$

$$c_4 = [S_1] \qquad c_5 = [S_1\,K] \qquad c_6 = [S_2] \qquad (2.1)$$
$$c_7 = [F] \qquad c_8 = [S_2\,F] \qquad c_9 = [S_1\,F]$$

to denote the species concentrations, under the assumption of mass action kinetics, one obtains the following reaction rates for the network (1.1),

$$r_1(k,c) = k_1\,c_1\,c_2, \qquad r_2(k,c) = k_2c_3, \qquad r_3(k,c) = k_3c_3, \qquad r_4(k,c) = k_4c_2c_4,$$
$$r_5(k,c) = k_5c_5, \qquad r_6(k,c) = k_6c_5, \qquad r_7(k,c) = k_7c_6c_7, \qquad r_8(k,c) = k_8c_8,$$
$$r_9(k,c) = k_9c_8, \qquad r_{10}(k,c) = k_{10}c_4c_7, \qquad r_{11}(k,c) = k_{11}c_9, \qquad r_{12}(k,c) = k_{12}c_9,$$

and the vector of reaction rates

$$r(k,c) = (r_1(k,c),\,\ldots,r_{12}(k,c))^T\ . \qquad (2.3)$$

In the ordering of (2.1) one obtains for the stoichiometric matrix:

$$\Gamma = \begin{bmatrix} -1 & 1 & 0 & 0 & 0 & 0 & 0 & 0 & 0 & 0 & 0 & 1 \\ -1 & 1 & 1 & -1 & 1 & 1 & 0 & 0 & 0 & 0 & 0 & 0 \\ 1 & -1 & -1 & 0 & 0 & 0 & 0 & 0 & 0 & 0 & 0 & 0 \\ 0 & 0 & 1 & -1 & 1 & 0 & 0 & 0 & 1 & -1 & 1 & 0 \\ 0 & 0 & 0 & 1 & -1 & -1 & 0 & 0 & 0 & 0 & 0 & 0 \\ 0 & 0 & 0 & 0 & 0 & 1 & -1 & 1 & 0 & 0 & 0 & 0 \\ 0 & 0 & 0 & 0 & 0 & 0 & -1 & 1 & 1 & -1 & 1 & 1 \\ 0 & 0 & 0 & 0 & 0 & 0 & 1 & -1 & -1 & 0 & 0 & 0 \\ 0 & 0 & 0 & 0 & 0 & 0 & 0 & 0 & 0 & 1 & -1 & -1 \end{bmatrix}. \qquad (2.4)$$

2.1. **The ODEs and PDEs derived from the mass action network.** Let t denote time. For network (1.1), the ODEs derived from formula (1.1) in the well mixed spatially homogeneous scenario read

$$\dot{c}_1 = -c_1(k_1c_2) + k_2c_3 + k_{12}c_9, \qquad (2.5a)$$
$$\dot{c}_2 = -c_2(k_1c_1 + k_4c_4) + k_2c_3 + k_3c_3 + (k_5 + k_6)c_5, \qquad (2.5b)$$
$$\dot{c}_3 = -c_3(k_2 + k_3) + k_1c_1c_2, \qquad (2.5c)$$
$$\dot{c}_4 = -c_4(k_4c_2 + k_{10}c_7) + k_3c_3 + k_5c_5 + k_9c_8 + k_{11}c_9, \qquad (2.5d)$$
$$\dot{c}_5 = -c_5(k_5 + k_6) + k_4c_2c_4, \qquad (2.5e)$$
$$\dot{c}_6 = -c_6(k_7c_7) + k_6c_5 + k_8c_8, \qquad (2.5f)$$
$$\dot{c}_7 = -c_7(k_{10}c_4 + k_7c_6) + (k_8 + k_9)c_8 + (k_{11} + k_{12})c_9, \qquad (2.5g)$$
$$\dot{c}_8 = -c_8(k_8 + k_9) + k_7c_6c_7, \qquad (2.5h)$$
$$\dot{c}_9 = -c_9(k_{11} + k_{12}) + k_{10}c_4c_7, \qquad (2.5i)$$

which together with initial conditions $0 < c_0 \in I\!R^9$ we abbreviate as

$$\dot{c} = \Gamma r(k,c),\ c(0) = c_0 \text{ with } c_0 > 0\ . \qquad (2.6)$$

Since $\Gamma r(k,c)$ is locally Lipschitz (for every positive k), by standard results from ODE theory there exists a time $T > 0$ (possibly infinite) and a unique solution $c \in C^1([0,T], I\!R^n_{>0})$. If the matrix Γ does not have full row rank, i.e. if $\mathrm{rank}(\Gamma) = s < n$, then there exists a matrix Z of maximal rank $n - s$ such that $Z^{'}\,\Gamma \equiv 0$. In this case, solutions $c(t)$ with initial value $c(0) = c_0$ satisfy

$$Z^{'}c(t) = Z^{'}c_0,$$

and the constant quantities $Z^{'}c_0$ are often referred to as total amounts, or total concentrations, total masses.

For network (1.1) and Γ as in (2.4) one finds $\operatorname{rank}(\Gamma) = 6$ and hence there exist 9×3-matrices Z such that $Z^{'}\,\Gamma \equiv 0$, for example the matrix

$$Z^{'} = \begin{bmatrix} 0 & 1 & 1 & 0 & 1 & 0 & 0 & 0 & 0 \\ 0 & 0 & 0 & 0 & 0 & 0 & 1 & 1 & 1 \\ 1 & 0 & 1 & 1 & 1 & 1 & 0 & 1 & 1 \end{bmatrix} .$$

Remark 2.1. If $\operatorname{rank}(\Gamma) = n - s$, then the Jacobian $J(c)$ of the function $\Gamma r(k, x)$ of a mass action network has at least s eigenvalues zero. Given a vector k and a steady state c we say that c is stable, if all eigenvalues that are not identically zero have negative real part. ⌋

In the spatially inhomogeneous scenario, the variables c are defined by solutions of the partial differential equation (PDE)

$$\partial_t c = \Gamma r(k, x) + D\,\Delta c, \tag{2.7a}$$

where D is a diagonal matrix containing the positive diffusion coefficients and Δ is the element-wise (negative) Laplace operator, i.e. $\Delta c_i = (\partial^2_{x_1} + \cdots + \partial^2_{x_d})c_i$, and the PDE is posed on some domain Ω with (piecewise) smooth boundary $\partial\Omega$ and Neumann (aka no-flux) boundary conditions

$$\partial_\nu c|_{x\in\partial\Omega} = 0, \tag{2.7b}$$

where ν is the outward unit normal and $\partial_\nu c$ the directional derivative, and with initial conditions,

$$c|_{t_0} = c_0 : \Omega \to \mathbb{R}^9_+. \tag{2.7c}$$

Though weaker notions of solution are possible, here solutions of (2.7) are functions

$$c : [0, T] \times \Omega \to \mathbb{R}^n_{>0}, (t, z) \mapsto (c_1(t, z), \ldots, c_n(t, z))^{'} ,$$

at least once differentiable in t and twice in x. Naturally, any solution $c : [0, T] \to \mathbb{R}^n_+$ of (2.6) satisfies the boundary conditions ((2.7)b) and hence can be identified with a spatially homogeneous solution of (2.7) to initial conditions $c_0(x) \equiv c_0$.

We are interested in steady solutions c^* of (2.6) and (2.7). Such steady states are called stable if (in the ODE case) for every $\varepsilon > 0$ there exists a $\delta > 0$ such that $\|c(0) - c^*\|_{\mathbb{R}^9} < \delta$ implies that the solution $c(t)$ exist for all $t > 0$ and $\|c(t) - c^*\|_{\mathbb{R}^9} < \varepsilon$ for all $t > 0$. Otherwise c^* is called unstable. For the PDE the notion of stability in principle depends on the chosen norms, but we can define $c^* : \Omega \to \mathbb{R}^9_+$ to be stable if $\|c(0, \cdot) - c^*(\cdot)\|_\infty < \delta$ implies that $c(t, \cdot)$ exists for all $t > 0$ and $\|c(t, \cdot) - c^*(\cdot)\|_\infty < \varepsilon$ for all $t > 0$. As explained above, we are in particular interested in the situation where a steady state $c^* \in \mathbb{R}^9$ is stable in the ODE, but the associated function $c^*(\cdot) \equiv c^*$ is unstable in the PDE, i.e., unstable wrt spatially inhomogeneous perturbations.

2.2. **Mass action networks that admit a monomial parametrization.** If a mass action network admits a monomial parametrization, then by [6, Lemma 3.5] there exists a set $\mathcal{K} \subseteq \mathbb{R}^r_{>0}$, a function $\psi : \mathcal{K} \to \mathbb{R}^n$ and a matrix $A \in \mathbb{R}^{p\times n}$ such that

$$\Gamma r(k, c) = 0 \Leftrightarrow k \in \mathcal{K} \text{ and } c = \psi(k) \circ \xi^A \text{ for some } 0 < \xi \in \mathbb{R}^p \text{ and } A \in \mathbb{R}^{n\times p}, \tag{2.8}$$

where $\circ$ denotes the element-wise product of two vectors, and $(\xi^A)_j = \prod_{i=1}^{p} \xi_i^{A_{ij}}$. One consequence of this equivalence is that for every $k \in \mathcal{K}$, one obtains infinitely many positive steady states (for that particular k) parameterized by ξ. Many signal transduction networks admit a monomial parametrization, for example the networks studied in [8, 9, 15, 25, 29] and some of the MESSI systems discussed in [28]. For an in-depth discussion see [6].

2.2.1. *A monomial parametrization for network (1.1).* By setting $(c_1, c_2, c_7) = (\xi_1, \xi_2, \xi_7)$ and setting (2.5a) – (2.5i) to zero and solving for c_3, c_4, c_5, c_6, c_8, c_9 we obtain the following parametrization of steady states for network (1.1):

$$(\xi_1, \xi_2, \xi_3) \mapsto (c_1, \dots, c_9) \tag{2.9a}$$

with

$$\begin{aligned} &c_1 = \xi_1,\ c_2 = \xi_2,\ c_3 = \frac{k_1}{k_2+k_3}\xi_1\xi_2,\ c_4 = \frac{k_1k_3(k_{11}+k_{12})}{k_{10}k_{12}(k_2+k_3)}\frac{\xi_1\xi_2}{\xi_3}, \\ &c_5 = \frac{k_1k_3k_4(k_{11}+k_{12})}{k_{10}k_{12}(k_2+k_3)(k_5+k_6)}\frac{\xi_1\xi_2^2}{\xi_3},\quad c_6 = \frac{k_1k_3k_4k_6(k_{11}+k_{12})(k_8+k_9)}{k_{10}k_{12}k_7k_9(k_2+k_3)(k_5+k_6)}\frac{\xi_1\xi_2^2}{\xi_3^2}, \\ &c_7 = \xi_3,\ c_8 = \frac{k_1k_3k_4k_6(k_{11}+k_{12})}{k_{10}k_{12}k_9(k_2+k_3)(k_5+k_6)}\frac{\xi_1\xi_2^2}{\xi_3},\ c_9 = \frac{k_1k_3}{k_{12}(k_2+k_3)}\xi_1\xi_2\ . \end{aligned} \tag{2.9b}$$

In this case the monomial parametrization is given by the following $\psi(k)$ and A:

$$\begin{aligned} \psi(k) = \Big(&1, 1, \frac{k_1}{k_2+k_3}, \frac{k_1k_3(k_{11}+k_{12})}{k_{10}k_{12}(k_2+k_3)}, \frac{k_1k_3k_4(k_{11}+k_{12})}{k_{10}k_{12}(k_2+k_3)(k_5+k_6)}, \\ &\frac{k_1k_3k_4k_6(k_{11}+k_{12})(k_8+k_9)}{k_{10}k_{12}k_7k_9(k_2+k_3)(k_5+k_6)}, 1, \frac{k_1k_3k_4k_6(k_{11}+k_{12})}{k_{10}k_{12}k_9(k_2+k_3)(k_5+k_6)}, \frac{k_1k_3}{k_{12}(k_2+k_3)}\Big), \end{aligned}$$

and

$$A = \begin{bmatrix} 1 & 0 & 1 & 1 & 1 & 1 & 0 & 1 & 1 \\ 0 & 1 & 1 & 1 & 2 & 2 & 0 & 2 & 1 \\ 0 & 0 & 0 & -1 & -1 & -2 & 1 & -1 & 0 \end{bmatrix}\ .$$

3. Turing–like instabilities

As described above, Turing's approach to pattern formation consists of two ingredients: a spatially homogeneous ODE of the form (2.6) and a reaction-diffusion PDE of the form (2.7), where the ODE has a stable steady state. This also defines a spatially homogeneous steady state solution of the PDE, and if the diffusion coefficients are such that this homogeneous steady state is unstable, then one speaks of Turing (–like) instability.

Throughout this section we will assume that our system admits a monomial parametrization of some positive steady states $\bar{c}$, suppressing the dependency on the k_i and ξ_i for notational simplicity. We will use the symbol $J(\bar{c})$ to denote the Jacobian of $\Gamma r(k, c)$ evaluated at $\bar{c}$, again suppressing the k_i-dependency for simplicity. We assume that $\bar{c}$ is (neutrally) stable in the ODE, i.e., that all nonzero eigenvalues of $J(\bar{c})$ have negative real parts and aim to identify conditions which yield that $\bar{c}$ is unstable in the PDE. For that we use the MP to derive the condition (1.2) after reducing the vector valued linearized problem to the lowest eigenvalues of the scalar Neumann Laplacian on Ω.

3.1. **Eigenvalues and determinants.** To identify Turing–like instabilities, the PDE (2.7) is linearized at the spatially homogeneous steady state $\bar{c}$. introducing $w(z,t) = c(z,t) - \bar{c}$, the local (i.e., linearized) dynamics are described by the linear PDE

$$\dot{w} = J(\bar{c})w + D\Delta w, \tag{3.1}$$

with Neumann BCs for w, and initial condition $w(0,z) = w_0(z)$. The stability of $w \equiv 0$ and hence of the homogeneous steady state $\bar{c}$ is then determined by the eigenvalues of the matrices

$$A_\ell = J(\bar{c}) - \mu_\ell D,\ \ell = 0, 1, 2, \dots \tag{3.2}$$

where μ_ℓ are the eigenvalues of the Neumann Laplacian $-\Delta$ on the domain Ω. In a first step we neglect the fact that A_ℓ is defined for the eigenvalues of $-\Delta$ and consider the matrix function

$$A(\mu) : I\!R \to I\!R^{n\times n},\ \mu \mapsto J(\bar{c}) - \mu D\ . \tag{3.3}$$

In a second step we identify values $\bar{\mu}$ for which the determinant $\det(A(\mu))$ has certain properties, and in a third step we combine this with conditions on the domain Ω that guarantee that there exist eigenvalues μ_ℓ of $-\Delta$ on Ω with $0 < \mu_\ell < \bar{\mu}$.

Lemma 3.1. *Let $A(\mu)$ be as in (3.3) where $J(\bar{c})$ and D are matrices of dimension $n \times n$ and satisfy $\operatorname{rank}(J(\bar{c})) = s < n$ and $D = \operatorname{diag}(d_1, \ldots, d_n)$ with $d_i > 0$. Then*

(i) With I_n is the $n \times n$-identity matrix, the determinant $\det(A(\mu))$ factors as

$$\det(A(\mu)) = \det(D)\, \det(J(\bar{c})D^{-1} - \mu I_n).$$

(ii) The determinant $\det(A(\mu))$ is equal to the characteristic polynomial of the matrix $J(\bar{c})D^{-1}$, up to the positive constant $\det(D)$.

(iii) The polynomial $\det(A(\mu))$ is not the zero polynomial.

Proof. (i) follows by a simple computation and the fact that D is a diagonal matrix with positive diagonal elements. (ii) follows directly from (i). Concerning (iii), we recall that right multiplication of a matrix with a diagonal matrix results in a rescaling of its column vectors. Hence right multiplication with such a diagonal matrix does not change its number of linear independent columns and hence its rank. Thus, $\operatorname{rank}(J(\bar{c})D^{-1}) = \operatorname{rank}(J(\bar{c})) = s > 0$ by assumption. Hence, in particular, the characteristic polynomial of $J(\bar{c})D^{-1}$ is not the zero polynomial. □

Corollary 3.2. *Let $\bar{\mu} \in \mathbb{R}$ be given. Then*

(i) $\det(A(\bar{\mu})) = 0$ if and only if $\bar{\mu}$ is an eigenvalue of $J(\bar{c})D^{-1}$.

(ii) If $\bar{\mu}$ is not an eigenvalue of $J(\bar{c})D^{-1}$, then all eigenvalues of $A(\bar{\mu})$ are nonzero.

Proof. (i) follows by Lemma 3.1(i) as by assumption $\det(D) \neq 0$. (ii) is a direct consequence of (i). □

Because the determinant of a matrix is equal to the product of its eigenvalues, the sign of $\det(A(\mu))$ can be used as an indicator for the existence of positive eigenvalues of the matrix $A(\mu)$:

Corollary 3.3 ($\operatorname{sign}(\det(A(\mu)))$ and positive eigenvalues of $A(\mu)$)**.**

(I) If μ is such that $\operatorname{sign}(\det(A(\mu))) = (-1)^{n+1}$, then
(a) the matrix $A(\mu) = J(\bar{c}) - \mu D$ has at least one positive eigenvalue and
(b) the number of positive eigenvalues of $A(\mu) = J(\bar{c}) - \mu D$ is odd.

(II) If μ is such that $\operatorname{sign}(\det(A(\mu))) = (-1)^n$, then the matrix $A(\mu) = J(\bar{c}) - \mu D$ has either no positive eigenvalues or an even number of such eigenvalues.

3.2. **Conditions for instabilities.** Lemma 3.1(iii) together with the $n - s$ conserved masses imply that the polynomial $\det(A(\mu))$ is of the form

$$\det(A(\mu)) = \det(D)\, \mu^{n-s} \left(a_0 \mu^s + \ldots + a_{s-1}\mu + a_s\right) \ . \tag{3.4}$$

If all eigenvalues of $A(\mu)$ have negative real part, then $\operatorname{sign}(\det(A(\mu)) = (-1)^n$. If an odd number of eigenvalues is positive, then $\operatorname{sign}(\det(A(\mu)) = (-1)^{n+1}$. As we do not want that $A(\mu)$ has positive eigenvalues for all positive values of μ, we want to have a sign change of the polynomial $\det(A(\mu))$ on the positive real line. The, arguably, algebraically easiest way to achieve this is a situation where the sign of the leading coefficient and of the constant coefficient are different. In this case $\det(A(\mu))$ will qualitatively look like the cartoons depicted in cf. Fig. 1 (or their negative). And for n odd, values of μ where $\det(A(\mu))$ is positive corresponds to $A(\mu)$ having positive eigenvalues (at least one). In case of n even, it is values of μ where $\det(A(\mu))$ is negative that correpond to $A(\mu)$ having positive eigenvalues.

Recall that the coefficients $a_0, \ldots, a_s$ are rational functions of the parameters k_i, d_i and ξ_i. In the following, we then assume that there exist parameter values, such that

$$\operatorname{sign}(a_0) = (-1)^n \tag{3.5a}$$

$$\operatorname{sign}(a_s) = (-1)^{n+1} \ , \tag{3.5b}$$

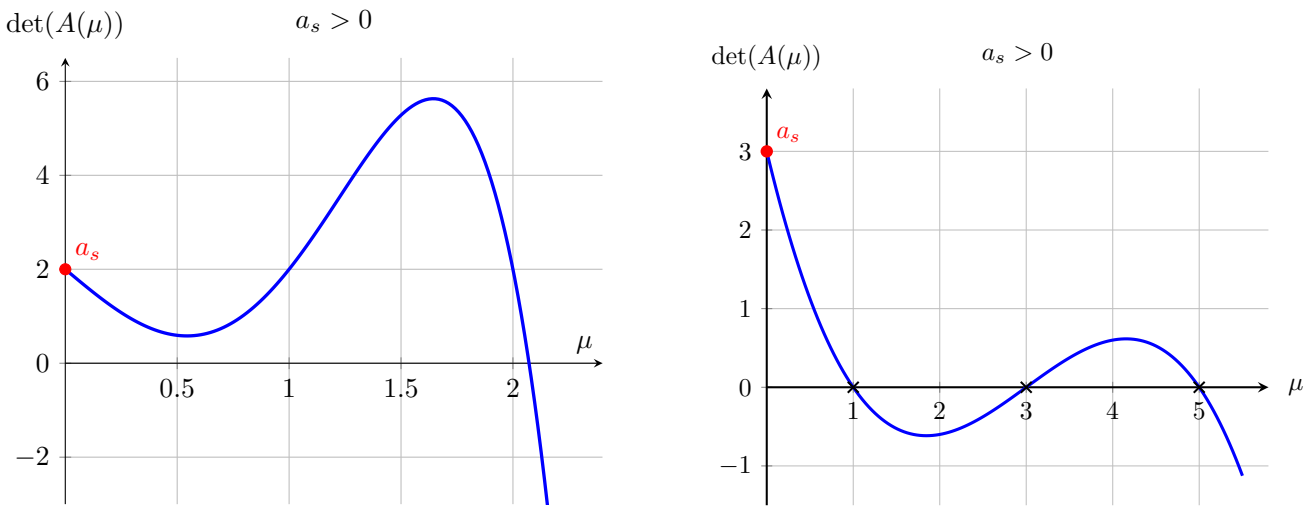

(A) One positive root (B) Three positive roots

FIGURE 1. Examples of polynomials with constant and leading coefficient of different sign that satisfy conditions (3.5a) & (3.5b) for n is odd (n even, corresponds to the negative of the depicted curves).

In this situation there exists (at least one) positive solution to $\det(A(\mu)) = 0$. Let $\bar{\mu}$ be the smallest positive zero of $\det(A(\mu)) = 0$. In the following theorem we note explicit conditions on the domain size $|\Omega|$ for $\mu_1 \in (0, \overline{\mu})$, and hence instability of $\bar{c}$, where μ_1 is the lowest positive eigenvalue μ_1 of the (positive) Neumann Laplacian $-\Delta$. These give guidance for the numerical analysis of the bifurcating branches in §4.

Theorem 3.4. *Recall the polynomial* $\det(A(\mu))$ *of (3.4) and let* k_i, d_i *and* ξ_i *be such that the coefficients* a_0 *and* a_s *satisfy (3.5a) & (3.5b). As above, let* $\bar{\mu}$ *be the smallest positive zero of* $\det(A(\mu))=0$. *Assume that* $\Omega \subset \mathbb{R}^d$, $d = 1, 2, 3$ *is simply connected with length, area, or volume* $|\Omega|$. *In this case there exists an eigenvalue* μ_ℓ *of the operator* $-\Delta$ *on* Ω *such that the corresponding matrix* $A_\ell = J(\bar{c}) - \mu_\ell D$ *has an odd number of positive eigenvalues (and at least one), if* $|\Omega|$ *satisfies*

$$d = 1 \ (\Omega \subset \mathbb{R} \text{ an interval}) : |\Omega| > \frac{\pi}{\sqrt{\bar{\mu}}}; \tag{3.6}$$

$$d = 2 \ (\Omega \subset \mathbb{R}^2): \quad |\Omega| > p_{1,1}^2 \frac{\pi}{\bar{\mu}}, \tag{3.7}$$

where $p_{1,1} \approx 1.8412$ *is first positive zero of the first derivative of the first Bessel function* J_1;

$$d = 3 \ (\Omega \subset \mathbb{R}^3): \quad |\Omega| > \frac{4}{3} p_{\frac{3}{2},1}^3 \frac{\pi}{(\bar{\mu})^{\frac{3}{2}}} \ . \tag{3.8}$$

where $p_{\frac{3}{2},1} \approx 2.0816$ *is first positive zero of the first derivative of* $x^{-\frac{1}{2}} J_{\frac{3}{2}}(x)$ *for the Bessel function* $J_{\frac{3}{2}}(x)$.

Proof. Assumptions (3.5a) and (3.5b) imply that $\operatorname{sign}(A(\mu)) = \operatorname{sign}(a_s)$ on $(0, \bar{\mu})$. By Corollary 3.3 this implies that for every $\mu \in (0, \bar{\mu})$ the corresponding matrix $A(\mu) = J(\bar{c}) - \mu D$ has at least one positive eigenvalue. Hence, if the lowest nontrivial eigenvalue μ_1 of $-\Delta$ on Ω lies in $(0, \bar{\mu})$, then the corresponding matrix $A_\ell = J(\bar{c}) - \mu_\ell D$ has an odd number of (and at least one) positive eigenvalues. For $d = 1$ we have $\mu_1 = \pi/|\Omega|$, yielding (3.6). For $d = 2$ and $d = 3$ the results follow by comparison with disks and balls (with again explicit eigenvalues), as by the isoperimetric inequality these yield

the largest first eigenvalues under given $|\Omega|$. In detail, for $d = 2$ we have $\mu_1 \leq p_{1,1}^2 \frac{\pi}{|\Omega|}$ [2, eq. (1.15)]), yielding (3.7), while $d = 3$ yields $\mu_1 \leq p_{\frac{3}{2},1}^2 \left(\frac{\frac{4}{3}\pi}{|\Omega|}\right)^{\frac{2}{3}}$ [2, eq. (1.15)], and hence (3.8). □

If $\bar{\mu}$ is the only positive root of $\det(A(\mu)) = 0$ we can sharpen Theorem 3.4:

Corollary 3.5. *In the setting of Theorem 3.4, let $\bar{\mu}$ be the only positive root of $\det(A(\mu)) = 0$. Then conditions (3.6) – (3.8) are necessary and sufficient for the existence of an eigenvalue μ_ℓ of $-\Delta$ on Ω such that the corresponding matrix A_ℓ has an odd number of positive eigenvalues (and at least one).*

Proof. By Theorem 3.4 conditions (3.6) – (3.8) are sufficient. To establish necessity let μ_ℓ be an eigenvalue of $-\Delta$ on Ω such that the corresponding matrix A_ℓ has an odd number of positive eigenvalues (and at least one). In this case $\operatorname{sign}(\det(A(\mu_\ell))) = \operatorname{sign}(a_s)$ by Corollary 3.3. As, by assumption, $\bar{\mu}$ is the only positive root and a_0 and a_s satisfy (3.5a) & (3.5b), it follows that $\operatorname{sign}(\det(A(\mu))) = \operatorname{sign}(a_s)$ if and only if $\mu \leq \bar{\mu}$ (cf. the general form of the polynomial $\det(A(\mu))$ in (3.4)). Hence we conclude $\mu_\ell \leq \bar{\mu}$. The properties of the eigenvalues of $-\Delta$ on Ω are such that $\mu_1 \leq \mu_\ell$ (see e.g. [17, Theorem 11.5.2] on the eigenvalues of $-\Delta$). Hence $\mu_1 < \bar{\mu}$ and conditions (3.6) – (3.8) follow by the same rearrangements as in the proof of Theorem 3.4. □

Based on Theorem 3.4, we can formulate the following condition concerning Turing-like instabilities:

Corollary 3.6. *Suppose there exist k_i, ξ_i and d_i such that a_0 and a_s satisfy (3.5a) & (3.5b). Further suppose that Ω is one of those discussed in Theorem 3.4. If the steady state $\bar{c}$ of the ODE (2.6) is such that all nonzero eigenvalues of the matrix $J(\bar{c})$ have negative real part, then Turing-like instabilities occur.*

Proof. By Theorem 3.4 there exists at least one eigenvalue μ_ℓ of the operator $-\Delta$ on Ω, such that the corresponding matrix $J(\bar{c}) - \mu_\ell D$ has an odd number of (and at least one) positive eigenvalues. As by assumption all nonzero eigenvalues $J(\bar{c})$ have negative real part the conditions for Turing-like instabilities described are satisfied. □

Remark 3.7. Let $\Omega \subset \mathbb{R}$ be a line segment with fixed length L and assume that $\bar{\mu}$ is the unique positive zero of $\det(A(\mu)) = 0$ (cf. Fig. 1b). Then, under the assumptions (3.5a) – (3.5b)) one has $\operatorname{sign}(\det(A(\mu))) = (-1)^{n+1}$ for $0 < \mu < \bar{\mu}$ and $\det(A(\mu)) = (-1)^n$ for $\mu > \bar{\mu}$. Since the eigenvalues of $-\Delta$ on Ω are given by $\mu_\ell = \left(\frac{\ell\pi}{L}\right)^2$, we can then determine L such that an arbitrary number of eigenvalues μ_ℓ is such that $\det(A(\mu_\ell)) > 0$ by rearranging the above formula. For each index ℓ with

$$1 \leq \ell \leq \left\lfloor \frac{\sqrt{\bar{\mu}}L}{\pi} \right\rfloor$$

one has $\det(A(\mu_\ell)) > 0$ and the corresponding matrix $J(\bar{c}) - \mu_\ell D$ has thus at least one positive eigenvalue (and always an odd number of such eigenvalues).

3.3. **Application to the double phosphorylation mechanism.** We now apply the above analysis to the network (1.1). We evaluate the Jacobian of the right hand side of (2.5a)–(2.5i) at (2.9b) to obtain $J(\bar{c})$ and compute $\det(J(\bar{c})D^{-1} - \mu I_9)$. This yields a degree nine polynomial in μ of the form

$$\mu^3(a_0\mu^6 + \cdots + a_5\mu + a_6) = 0,$$

where the a_i are rational functions of the k_i, d_i and ξ_i. All terms in the common denominator of the a_i have positive sign, hence the common denominator of the a_i is positive for positive values of k_i, d_i and ξ_i. Consequently, in light of Theorem 3.4 the signs of the numerators of the coefficients a_0 and a_6 are of interest. We note the following facts:

Fact 1: All terms in the numerator of a_0 have negative sign, hence a_0 is negative for all positive values of the k_i, d_i and ξ_i.

Fact 2: The numerator of a_6 as a polynomial in ξ_1 is of degree two (in ξ_1) that factors as

$$\text{Numerator}(a_6) = (d_3d_8k_{12}k_6 - d_5d_9k_3k_9)\,\gamma_0\xi_1^2 + \gamma_1\xi_1 + \gamma_2,$$

where γ_0, γ_1 and γ_2 are polynomials in the k_i, d_i and ξ_2 and ξ_3.

Fact 3: The coefficient γ_2 contains only negative terms, γ_1 contains positive and negative terms and γ_0 contains only positive terms.

To further discuss a_6 as a function of ξ_1 we use the symbol $a_6(\xi_1)$.Note that for arbitrary positive values of the k_i and d_i that satisfy (3.9) and arbitrary positive ξ_2, ξ_3 the signs of the terms in γ_0 and γ_2 imply that $a_6(\xi_1)$ is a quadratic polynomial in ξ_1 with negative constant coefficient. Thus, we observe:

Fact 4: If

$$d_3d_8k_{12}k_6 - d_5d_9k_3k_9 > 0, \tag{3.9}$$

then there exist a unique positive value $\bar{\xi}_1$ such that $a_6(\bar{\xi}_1) = 0$.

Fact 5: This unique positive zero $\bar{\xi}_1$ of $a_6(\xi_1)$ is such that

$$a_6(\xi_1) < 0 \text{ for } 0 < \xi_1 < \bar{\xi}_1 \text{ and } a_6(\xi_1) > 0 \text{ for } \xi_1 > \bar{\xi}_1\ .$$

This leads to the final conclusion:

Fact 6: If k_i, d_i satisfy (3.9) and if $\xi_1 > \bar{\xi}_1$, then the coefficients a_0 and a_6 of $\det(J(\bar{c}) - \mu D)$ satisfy the conditions (3.5a) & (3.5b) and we are in the situation of Theorem 3.4.

Lemma 3.8 (Eigenvalues μ_ℓ of $-\Delta$ and positive eigenvalues of $J(\bar{c}) - \mu_\ell D$ for appropriate Ω)**.** *Pick k_i and d_i such that*

$$\frac{k_3k_9}{k_6k_{12}} < \frac{d_3d_8}{d_5d_9}\ . \tag{3.10}$$

Fix $\xi_2 > 0$ and $\xi_3 > 0$, let $\bar{\xi}_1$ be the unique positive solution to $a_6(\xi_1) = 0$ and pick $\xi_1 > \bar{\xi}_1$. Determine $\bar{c}$ according to (2.9b).
If Ω is as in Theorem 3.4, then the operator $-\Delta$ has an eigenvalue μ_ℓ such that the corresponding matrix $J(\bar{c}) - \mu_\ell D$ has an odd number of positive eigenvalues (and at least one).

Proof. Inequality (3.10) is equivalent to (3.9) and as explained in Fact 1 – 6 this implies that the k_i, d_i and ξ_i are such that the coefficients a_0 and a_6 of $\det(J(\bar{c})D^{-1} - \mu I_6)$ satisfy the assumptions (3.5a) & (3.5b). Hence, by Theorem 3.4 the domain Ω can be chosen such that there exists an eigenvalue μ_ℓ of the operator $-\Delta$ such that the matrix $J(\bar{c}) - \mu_\ell D$ has and odd number of positive eigenvalues (and at least one). □

The ODEs derived from network (1.1) can admit multistationarity [5], that is, there may be at least two positive steady states for some values of the total amounts. We expand on this in the following remark.

Remark 3.9. [Multistationarity in the ODE system of network (1.1)] As discussed in §2.1, in the ODE setting the solutions $c(t)$ are confined to the affine subspaces $Z^{'}c = Z^{'}c_0$ (where $c(0) = c_0$), i.e., with masses $m = m(c_0)$. This has important implications when talking about the number of steady states: Given a monomial parametrization, there exists an infinite number of steady states. But given an initial condition $c_0 > 0$ only a limited number of steady states is of interest, those with $m(\bar{c}) = m_0$.

More formally, let $\bar{c}(\xi)$ be the steady state parametrization (suppressing the k_i dependency for notational simplicity) and let m_0 be given. Then only those elements of $\bar{c}(\xi)$ contained in the affine subspace $Z^{'}c = Z^{'}c_0$ are relevant for the solution $c(t)$ with $c(0) = c_0$. These are defined by the positive solutions of

$$Z^{'}\bar{c}(\xi) = Z^{'}c_0\ .$$

If there are ≥ 2 such positive solutions, then one speaks of multistationarity, and if ≥ 2 such steady states are locally dynamically stable, then of multistability. In [7] it has been shown, that if the rate constants of network (1.1) satisfy

$$k_3k_9 - k_{12}k_6 < 0, \tag{3.11}$$

then there exists $\bar{\xi}_1$ (for every fixed positive $\bar{\xi}_2$ and $\bar{\xi}_3$) such that the equation

$$Z'\bar{c}(\xi) = Z'\bar{c}(\bar{\xi})$$

has three positive solutions [7, Theorem 5.1&Corollary 5.1]. Here the steady state $\bar{c}(\bar{\xi})$ takes on the role of the vector c_0 in defining the affine subspace. In the numerical examples in §4 we see the multistationarity condition (3.11) approximately, as we do not aim for sharp $\bar{\xi}_1$, see Figures 3 and 4, and Footnote 4. ⌋

4. Numerical examples

4.1. **General remarks and setup.** We use the numerical continuation and bifurcation package `pde2path` [35, 27] to first continue steady states and some time-periodic orbits (POs) of the reaction–diffusion PDE (2.7), i.e.,

$$\partial_t c = G(c) := f(c) + D\Delta c, \quad f(c) = \Gamma r(k,c), \quad D = \mathrm{diag}(d_1,\dots,d_9), \tag{4.1}$$

on domains $\Omega = (-l,l) \subset I\!R$ (1D interval) or Ω_R (disk of radius R) with Neumann BCs. Subsequently we will also run some numerical time integration, aka direct numerical simulation (DNS). We throughout fix the "base parameter set"

$$(d_1,d_2,d_3,d_4,d_5,d_6,d_7,d_8,d_9) = (0.1,0.3,2,0.4,0.5,0.02,0.8,0.5,0.5), \text{ and} \tag{4.2a}$$

$$(k_1,k_2,k_4,k_5,k_6,k_7,k_8,k_9,k_{10},k_{11},k_{12}) = (1,0.3,4.2,1.6,1,0.1,2.2,0.5,0.5,0.8,1), \tag{4.2b}$$

and use $k_3 > 0$ as a bifurcation parameter, and $\bar{c}(\xi)$ with $(\xi_1,\xi_2,\xi_3) = (1,1,2)$ as a starting point for the continuation. Additionally, we use (4.2) with k_9 changed to

$$k_9 = 1, \tag{4.3}$$

because in this case the primary loss of stability of $\bar{c}$ is due to Hopf bifurcations.

The steady state continuation and bifurcation requires to explicitly implement as constraints the mass conservations

$$\frac{\mathrm{d}}{\mathrm{d}t} m_i = 0, \tag{4.4}$$

$m_1 = \langle c_2 + c_3 + c_5\rangle,\ m_2 = \langle c_7 + c_8 + c_9\rangle,\ m_3 = \langle c_1 + c_3 + c_4 + c_5 + c_6 + c_8 + c_9\rangle$, where $\langle c\rangle = \frac{1}{|\Omega|}\int_\Omega c\,\mathrm{d}x$, because for numerical continuation and bifurcation we must get rid of the three 0 eigenvalues associated to (4.4) (see [35, §3.5] for general background on continuous symmetries and constraints in `pde2path`). For this, there are basically two options: Either we choose

$$q(c) := \begin{pmatrix} q_1(c) \\ q_2(c) \\ q_3(c) \end{pmatrix} := \begin{pmatrix} \langle c_2 + c_3 + c_5\rangle - m_1(k_3) \\ \langle c_7 + c_8 + c_9\rangle - m_2(k_3) \\ \langle c_1 + c_3 + c_4 + c_5 + c_6 + c_8 + c_9\rangle - m_3(k_3) \end{pmatrix} = \begin{pmatrix} 0 \\ 0 \\ 0 \end{pmatrix}, \tag{4.5}$$

with $m_j(k_3)$ given from the monomial parametrization (MP) (2.9b) of that specific homogeneous branch, or

$$q(c) := \begin{pmatrix} q_1(c) \\ q_2(c) \\ q_3(c) \end{pmatrix} := \begin{pmatrix} \langle c_2 + c_3 + c_5\rangle - m_1 \\ \langle c_7 + c_8 + c_9\rangle - m_2 \\ \langle c_1 + c_3 + c_4 + c_5 + c_6 + c_8 + c_9\rangle - m_3 \end{pmatrix} = \begin{pmatrix} 0 \\ 0 \\ 0 \end{pmatrix}, \tag{4.6}$$

with $m = (m_1,m_2,m_3)$ set at initialization. The MP variant is close to the analysis and explicitly based on the homogeneous branch (2.9b), and only allows bifurcations from this with $m = m(k_3)$. We use this in Figures 3 and 4. The second variant can be considered as constraints given by initial

conditions (of the continuation), and hence yields bifurcation diagrams (in k_3 or any other parameter) at fixed m throughout. For brevity we call this a "natural parametrization" (NP), and use this in Figures 6 and 7.

In both cases, to implement the constraints (4.5) or (4.6) we introduce three Lagrange–multipliers $\varepsilon_1, \varepsilon_2, \varepsilon_3$ and obtain the modification

$$\widetilde{f}(c) = (f_1+\varepsilon_3, f_2+\varepsilon_1, f_3+\varepsilon_1+\varepsilon_3, f_4+\varepsilon_3, f_5+\varepsilon_1+\varepsilon_3, f_6+\varepsilon_3, f_7+\varepsilon_2, f_8+\varepsilon_2+\varepsilon_3, f_9+\varepsilon_2+\varepsilon_3), \tag{4.7}$$

which we directly rename to f. When solving $G(c) = 0$ with (4.5) or (4.6) with the new f we then want the ε_i to stay zero (numerically $\mathcal{O}(10^{-12})$, say), which they do.

When considering (4.1) on a disk, we have a continuous rotational symmetry (see also Remark 4.1): In polar coordinates $x = r(\cos\phi, \sin\phi)$, if $c(r, \phi)$ is a steady state, so is $c(r, \phi + \vartheta)$ for any $\vartheta \in I\!R$. Hence, if $\partial_\phi c \not\equiv 0$, then $\partial_\phi c$ is in the kernel $N(\partial_c G)$ of $\partial_c G$, yielding a fourth 0 eigenvalue. To remove this, we go into a co–rotating frame $\vartheta = \phi - st$, which modifies (4.1) to

$$\partial_t c = G(c) + s\partial_\phi c, \tag{4.8}$$

with the speed s a priori unknown. To continue solutions of (4.8), additional to k_3 we "free" the parameter s and then need to add the rotational phase condition (PC)

$$\langle \partial_\phi u, u_0 \rangle = 0, \tag{4.9}$$

where u_0 is a reference solution, usually from the previous continuation step.[1] [2] Steady states of (4.8) with $s = 0$ are genuine steady states of (4.1), and steady states of (4.8) with $s \neq 0$ (so called relative equilibria) correspond to states rotating in (4.1) with angular speed s, so called rotating waves (RWs), and as we shall see these RWs play a prominent role in (4.1) over disk domains.

Remark 4.1. We collect a number of Remarks on the spectra and eigenfunctions of $\partial_c G(\bar{c})$ on intervals and disks with Neumann BCs as already used in Theorem 3.4, and on the "symmetry perspective" [12, 13, 16] on bifurcations from homogeneous steady states $\bar{c}$.

a) Over $I\!R$, the eigenfunctions of $\partial_c G$ have the form of *Fourier modes* $V(x;\kappa) = \mathrm{e}^{\mathrm{i}\kappa x}\hat{V}(\kappa)$ where $\kappa \in I\!R$ is called the wave number, and $\hat{V}(\kappa) \in \mathbb{C}^9$ is an eigenvector of $A(\kappa) := J(\bar{c}) - \kappa^2 D$. For any $\kappa \in I\!R$, $A(\kappa) \in I\!R^{9\times 9}$ has 9 (counted with multiplicity) eigenvalues $\mu_1(\kappa), \ldots, \mu_9(\kappa) \in \mathbb{C}$, and we define the curves $\kappa \mapsto \mu_j(\kappa)$ by sorting wrt decreasing real parts. We can then numerically compute and plot the *dispersion relations* (DRs), i.e., the leading eigenvalue curves $\kappa \mapsto \mu_j(\kappa)$, $j = 1, 2, 3$, say, as in Fig.3(a,b) and Fig.4(a,b).

Over bounded intervals with Neumann BCs, i.e., $\Omega = (-l, l)$, only wave numbers $\kappa = \kappa_m = m\pi/(2l)$ are allowed. Moreover, (4.1) is Z_2 equivariant, i.e., invariant under $x \mapsto -x$. Therefore:

- All steady state BPs from $\bar{c}$, i.e., $\mu_j(\kappa_m) = 0$ for some j, are generically simple, with kernels of the form $V(x) = \sin(m\pi x/(2l))\hat{V}_m$, $\hat{V}_m \in I\!R^9$, $m \in \mathbb{N}$ odd, or $V(x) = \cos(m\pi x/(2l))\hat{V}_m$, $m \in \mathbb{N}$ even. For $m \neq 0$ the bifurcating branches are necessarily pitchforks due to the "hidden symmetry" of shifting the solution by half a spatial period. However, for $m = 0$ we shall find a transcritical bifurcation of a second homogeneous branch $\tilde{\bar{c}}$ from $\bar{c}$, at "small" k_3. This should be expected from the multistationarity condition (3.11), see Footnote 4.
- We have Hopf bifurcation points if a pair of complex conjugate eigenvalues $\mu_j = \overline{\mu_{j+1}}$ with $\mathrm{Im}(\mu_j) \neq 0$ crosses the imaginary axis, see for instance Fig.4(a,b). In 1D with NBCs, this yields the pitchfork bifurcations of so called standing waves, i.e., time periodic orbits with discrete points x_j where $c(t, x_j)$ oscillates with maximal amplitude. See Fig.4 for examples, where however we only briefly look at such SWs because their computation is quite demanding numerically, and the SWs obtained are all unstable, possibly with some exception in a narrow parameter regime. Instead we will focus on RWs in 2D, see Fig.7. The analog of RWs in 1D

[1] More formally, this makes the continuation orthogonal to the group orbit of rotations, again see [35, §3.5] for general background, or [35, Part II] or [30] for simple examples.

[2] See also [3] for the `Matlab` sources of our implementation, together with a reference sheet and further plots.

would be traveling waves (TWs), which for instance would bifurcate for periodic boundary conditions together with the SWs, but here the TWs are prohibited by the Neumann BCs.

b) The eigenfunctions of the (scalar) Neumann Laplacian on disks D_R of radius R are

$$v(r,\phi) = b(r)\mathrm{e}^{\mathrm{i}m\phi}, \quad m = 0, 1, \ldots, \tag{4.10}$$

where $b(r) = J_m(s'_{mn}r/R)$ with J_m the mth Bessel function of the first kind and $s'_{mn} = n$–th zero of $J'_m(r)$, and m is called azimuthal wave number. We thus label the eigenfunctions as $v_{mn}(r,\phi)$, with eigenvalues $\mu_{mn} = (s'_{mn}/R)^2$, cf. Theorem 3.4. For the (complexified) vector valued linearized problem $G_c(\overline{c})V = \mu V$, $V \in L^2(\Omega, \mathbb{C}^9)$, the eigenfunctions have the form

$$V(r,\phi) = v_{mn}(r,\phi)\hat{V}_{mn} \text{ with } \hat{V}_{mn} \in \mathbb{C}^9.$$

The rotational invariance of (4.1) on disks yields that the problem is $O(2)$ equivariant, i.e., invariant under $\phi \mapsto -\phi$ and under $\phi \mapsto \phi + \vartheta$, $\vartheta \in \mathbb{R}$. Therefore:

- Steady state BPs with kernels $N(\partial_c G(\overline{c}))$ with angular dependency ($m \neq 0$) come with multiplicity at least two, i.e., $v_{mn}(r,\phi)\hat{V}_{mn}$ and $v_{mn}(r,\phi+\pi/2)\hat{V}_{mn}$ are two linearly independent eigenfunctions. Moreover, all bifurcations of this type must be pitchforks due to the "hidden" symmetry $\phi \mapsto \phi + \pi/2$. For $m = 0$ ("Mexican hats") the BPs are generically simple, and we expect transcritical bifurcations of such branches.
- For Hopf bifurcations with $m \neq 0$ we automatically have three bifurcating branches: clockwise ($s < 0$ in (4.8)) and counterclockwise ($s > 0$ in (4.8)) RWs, RW_+ and RW_- for short, and again SWs as equal amplitude superpositions of $\mathrm{RW}_\pm$. We refrain from computing SWs in 2D, but in §4.4 we compute branches of 2D RWs.

Remark 4.2. a) Inspection of the DRs in Fig.3(a,b), and of similar DRs in various other parameter regimes, yields that the instabilities of $\overline{c}$ wrt modes $V(x;\kappa)$ with $\kappa \neq 0$ is of *long wave* (or *sideband*) type, as analyzed in Theorem 3.4. That means that the instability sets in by a change of curvature of the critical eigenvalue curve $\kappa \mapsto \mu_1(\kappa)$ at $\kappa = 0$. We have $\mu_1(0) = 0$ (and $\mu_2(0) = \mu_3(0) = 0$ for all parameters due to the mass conservations), $\mu'_j(0) = 0$ for $j = 1, \ldots, 9$ due to the reflection symmetry $x \mapsto -x$, and $\mathrm{Re}\mu_j(\kappa) \sim -\kappa^2$ for $\kappa \to \infty$ and $j = 1, \ldots, 9$. Moreover $\mathrm{Re}\mu''_1(0) < 0$ for $k_3 > k_{3,c} \approx 4.49$, and $\mathrm{Re}\mu''_1(0) > 0$ for $k_3 < k_{3,c}$, yielding $\mathrm{Re}\mu_1(\kappa) > 0$ in a small interval $(0, \kappa_0)$.

In this situation, over finite intervals $(-l, l)$, the first mode to become unstable always is the one with minimal wave number $\kappa_1 = \pi/(2\ell)$, followed by the second mode $\kappa_2 = \pi/\ell$, and so on. Therefore, these instabilities are called Turing–like, while genuine Turing instabilities are of finite wave number type, i.e., the critical wave number κ_c (defined over $\mathbb{R}$) is of order 1.

b) Similar remarks also apply to the 2D case, where analogs of Fig.3(a,b) can also be computed, yielding (punctured) disks $\{\kappa = (\kappa_1, \kappa_2) : |\kappa| < \kappa_0, \kappa \neq 0\}$ of unstable wave vectors, respectively for finite domains discretization of these, for instance according to (4.10), and over disks we then find the order of instabilities as $(m, n) = (1, 1), (2, 1), (0, 1), \ldots$.

c) Examples of genuine Turing instabilities (κ_c=$\mathcal{O}(1)$) and Turing–Hopf instabilities ($\mathrm{Re}\mu_1(\kappa_c)$=0 and $\mathrm{Im}\mu_1(\kappa_c) \neq 0$) in systems with conserved quantities can be found in, e.g., [22] (for the conserved Swift–Hohenberg equation as a model problem), and [14, 38, 23]. In order to find genuine Turing instabilities for (4.1), besides using the base parameter set (4.2) we numerically computed DRs for various different parameter combinations, in particular varying the diffusion constants from (4.2b). This was mainly based on intuition, trying to find activator and inhibitor groups as in [31], but without success, i.e., in all cases the instabilities were of long wave sideband type. Thus, finding genuine Turing instabilities for (4.1) (and possibly associated wave instabilities with $\mathrm{Re}\mu_1(\kappa_c) = 0$ and $\mathrm{Im}\mu_1(\kappa_c) \neq 0$) remains an interesting open problem. ⌋

4.2. **Numerical evaluation of the analytical instability predictions.** For the base parameter set (4.2), the conditions (3.10) and (1.2) evaluate to $\frac{k_3 k_9}{k_6 k_{12}} = \frac{k_3}{2}$ and $\frac{d_3 d_8}{d_5 d_9} = 4$, i.e., $2 < k_3 < 8$, and for

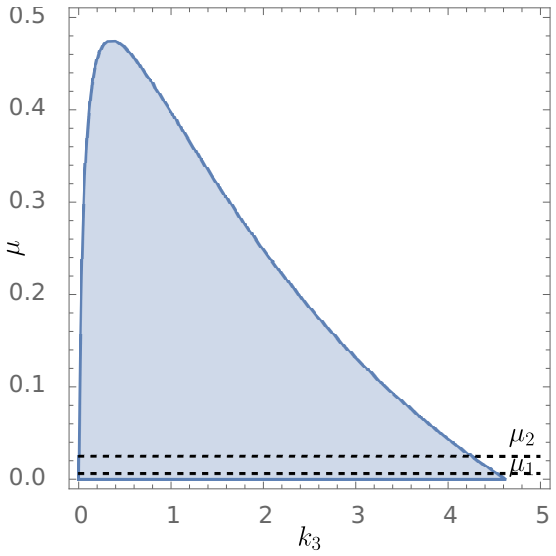

FIGURE 2. Shaded region: values of k_3 and μ with $\det(A(\mu)) > 0$.

(4.3) to $1 < k_3 < 4$. In light of Facts 4 and 5 on page 10 we investigate $\det(A(\mu))$ and the coefficient a_6, namely

$$\begin{aligned}\det(A)(\mu) &= C\mu^3(a_0\mu^6 + \ldots + a_5\mu + a_6)\\ &= \frac{\mu^3}{(k_3+0.3)^2}\Big[-\left(0.000048k_3^2 + 0.0000288k_3 + 4.32\cdot 10^{-6}\right)\mu^6\\ &\quad -\left(0.000024k_3^3 + 0.01113k_3^2 + 0.00402467k_3 + 0.000206352\right)\mu^5\\ &\quad -\left(0.00539418k_3^3 + 0.716149k_3^2 + 0.105762k_3 + 0.00356709\right)\mu^4\\ &\quad -\left(0.339791k_3^3 + 9.28858k_3^2 + 1.02013k_3 + 0.0268889\right)\mu^3\\ &\quad -\left(4.4146k_3^3 + 33.5369k_3^2 + 3.46057k_3 + 0.0846663\right)\mu^2\\ &\quad -\left(15.4912k_3^3 + 16.2052k_3^2 + 2.95065k_3 + 0.0910211\right)\mu\\ &\quad -5.6007k_3^3 + 25.6708k_3^2 + 0.922778k_3 - 0.00472212\Big].\end{aligned} \tag{4.11}$$

For positive k_3, all coefficients are negative, except

$$a_6(k_3) = -5.6007k_3^3 + 25.6708k_3^2 + 0.922778k_3 - 0.00472212$$

which is positive for $0.00454356 < k_3 < 4.61914$. As a_0 is negative for all positive values of k_3, the coefficients of the polynomial (4.11) satisfy the assumption (3.5a) & (3.5b) for values of k_3 in the above interval. We can thus apply Corollary 3.2 and Theorem 3.4. By Corollary 3.3 eigenvalues μ_ℓ of $-\Delta$ such that $\det(A(\mu_\ell)) > 0$, yield instabilities, and in summary we find that $\det(A(\mu)) > 0$ for the values depicted in Fig. 2. For $\Omega = (-l, l)$ with $l = 20$ as in §4.3, $\mu_1 = \pi^2/(2l)^2 \approx 0.0062$, $\mu_2 \approx 0.0247$, and inspecting the associated lines in Fig.2 indeed yields good predictions for the k_3 values for the bifurcations of these modes from $\bar{c}$.

4.3. **1D.** Fig.3(a,b) show DRs (cf. Remark 4.1a)) for linearizations of (4.1) around the homogeneous steady states $\bar{c}(k_3)$ from (2.9b), with parameters from (4.2). These show that the primary instability of $\bar{c}(k_3)$ is at some $k_3 = k_{3c} \in (4, 4.5)$ ($k_{3c} \approx 4.48$) and is of steady long wave type. Even though the eigenvalues μ with small $|\mathrm{Re}(\mu)|$ are in general complex, the instability onset is for real eigenvalues, as illustrated in (b), and altogether there are no Hopf bifurcations at all from $\bar{c}$ in this regime. (This is different in Fig.4 for $k_9 = 1$, where there are several Hopf bifurcations from $\bar{c}$, including the primary loss of stability).

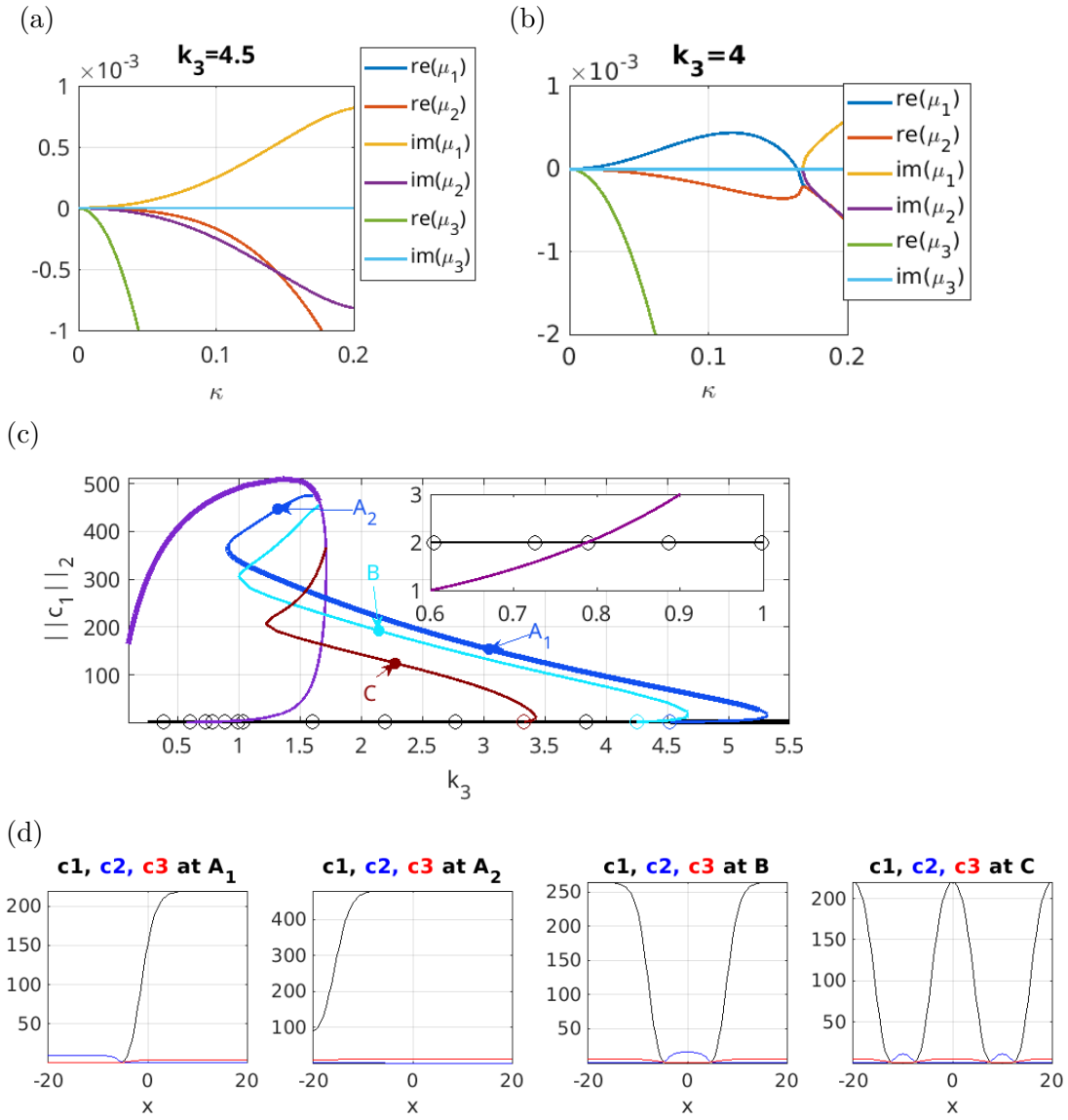

FIGURE 3. Parameters (4.2), constraints $m = m(k_3)$ based on (2.9b) (MP setting), continuation in k_3. (a,b) Dispersion relations before and after spatial instability of $\bar{c}(k_3)$. (c,d) Basic bifurcation diagram, and sample solutions.

Fig.3(c) shows a basic BD for (4.1), (4.5) on $\Omega = (-20, 20)$ with Neumann BCs[3], where

$$\|c_1\|_2 := \left(\frac{1}{|\Omega|} \int_\Omega c_1^2(x)\, \mathrm{d}x \right)^{1/2}. \tag{4.12}$$

This is not a norm, as it uses only the first component of $c \in L^2(\Omega, I\!R^9)$, but motivated by the fact that $c_1(k_3) = \xi_1$ independent of k_3 in the MP setting. Similarly, in the sample plots in (d) we restrict to the first three components of c, and refer to [3] for plotting other components.

Thicker lines in (c) indicate stable (parts of) branches, and branch points from the black branch $k_3 \mapsto \bar{c}(k_3)$ with $\|c_1\|_2 \equiv \xi_1 = 2$ are indicated by $\circ$. We show the 1st ("A" branch, blue), 2nd ("B" branch, light blue), and 4th ("C" branch, brown) patterned branches bifurcating from $\bar{c}$. All these bifurcations are subcritical pitchforks (meaning that they initially go into direction of "more stable" $\bar{c}$, i.e., towards larger k_3), with a turning point (fold) shortly after bifurcation. In particular, the primary patterned branch A is unstable at bifurcation but stabilizes shortly after its right fold. Additionally we have a second homogeneous branch $\widetilde{\bar{c}}$ (violet) bifurcating transcritically (see inset)

[3]we refer to Remark 4.3 and [3] for details on the spatial discretization

from $\overline{c}$ at $k_3 \approx 0.8$, which for initially increasing k_3 shows a fold at $k_3 \approx 1.9$ and then stabilizes after reconnection of the A branch at $k_3 \approx 1.8$.[4]

Similarly, also the other patterned branches connect $\overline{c}$ and $\widetilde{\overline{c}}$. Thus, besides the multistationarity of $\overline{c}$ and various patterned branches for $k_3 < k_{3,c}$, we also have multistationarity of two homogeneous branches for $k_3 < 1.9$. Moreover, we have different multistabilities, namely of $\overline{c}$ and A for $k_3 > k_{3c}$ and of $\widetilde{\overline{c}}$ and A for $k_3 \in (0.9, 1.8)$ (left fold of A and reconnection of A to $\widetilde{\overline{c}}$).

In Fig.4 we illustrate that besides the steady state bifurcations as in Fig.3, (4.1) can also show Hopf bifurcations. Namely, for $k_9 = 1$, the primary instability of $\overline{c}$ is at $k_3 \approx 2.82$ and is of long wave Hopf type, with small imaginary parts, see (a). Subsequent bifurcations from $\overline{c}$ then also include the steady long wave type, see (b) for the DR at smaller k_3. In the main BD in (c) we focus on steady branches, which we plot with the same colors as in Fig.3, and which behave completely analogous, and thus we omit samples here. The inset of (c) shows in more detail the behavior at loss of stability of $\overline{c}$, including the first SW branch (orange, samples in (d)), and a "breather" branch (green, samples in (f)) which bifurcates from the A branch yielding gain of stability of A. Here,

$$\|c_1\|_2 := \left(\frac{1}{|\Omega| T} \int_0^T \int_\Omega c_1^2(t,x) \, \mathrm{d}x \, \mathrm{d}t \right)^{1/2} \tag{4.13}$$

generalizes (4.12) to T periodic solutions. The behavior of T along the SW and the breather branches is shown in (e). The SW branch again bifurcates subcritically (to increasing k_3), and along the branch, T first decreases and then increases again. At the maxima of the amplitudes (at $x = \pm l$) the oscillations quickly develop into a rather strong relaxation type, which makes the continuation of the SW branch to large amplitude numerically expensive due to the fine t discretization of up to 200 points needed, and the same holds for the breather branch.

Remark 4.3. a) For the computation of Fig. 3(c) and Fig.4(c) we use piecewise linear finite elements in space with a rather moderate discretization of 100 mesh points, because of the rather fine meshes in t of up to 200 points needed for the computation of SWs. Due to the 9 components of c, this yields $9 \times 100 \times 200 = 180000$ degrees of freedom (DoF) altogether, and the continuation of the SW and breather branches in Fig. 4(c) needs about 1h on a laptop computer. In contrast, the computation of all the steady branches in Fig.3(c) and Fig.4(c) only needs a few minutes. Moreover, we checked that all the steady state results remain unchanged for double the resolution, i.e., 200 spatial points, hence 1800 spatial DoF.

b) There are further Hopf points on the spatially inhomogeneous branches, and the bifurcating branches generally lead to "breathing peaks". However, none of these appear to be stable, as discussed via DNS next, and therefore we restrict to the green branch, which is also the most interesting as its bifurcation leads to the gain of stability of the A branch. ⌋

The stability of SWs (of time periodic orbits in general) can be analyzed via their Floquet multipliers, which also determine the bifurcations *from* time periodic orbits such as period doubling or torus bifurcations, [35, §3.4]. However, the numerical computation of the Floquet multipliers is a difficult and expensive task and often prone to numerical instabilities, in particular for relaxation oscillation type of solutions as in Fig.4. Therefore, to illustrate (in)stability of the SWs, in Fig. 5 we run time integration (aka direct numerical simulation DNS) from (perturbations of) selected SWs. That means we let $\tilde{c}(x) = c_{\mathrm{SW}}(0,x)$ (time $t = 0$ slice) and add $0.1\cos(\pi x/20)$ to the first component of $\tilde{c}$ (which does not change the masses m), to obtain a perturbed initial condition for the DNS.

Fig.5(a-c) shows the result of doing so for SW_2 (see [3] for the DNS method used, i.e., linearly implicit Euler). (a) shows a space–time plot of c_1, (b) a snapshot of c_1 (and c_2 and c_3) at the stopping time, and (c) the "residual" $\|G(t)\|_\infty$, i.e., the amplitude of the dynamics. This again shows the

[4]This behavior agrees with the multistationarity condition (3.11). For the parameter set (4.2), $k_{3\mathrm{mult}} := k_6 k_{12}/k_9 = 2$, and we should expect the bifurcation of the $\widetilde{\overline{c}}$ branch at some $k_3 < k_{3\mathrm{mult}}$, and $\widetilde{\overline{c}}$ to extend to roughly $k_{3\mathrm{mult}}$, but with in general the fold at some $k_{3f} < k_{3\mathrm{mult}}$; this is because we do not vary ξ_1 here, i.e., do not search for the "optimal" $\bar{\xi}_1$ to yield multistationarity for k_3 near $k_{3\mathrm{mult}}$.

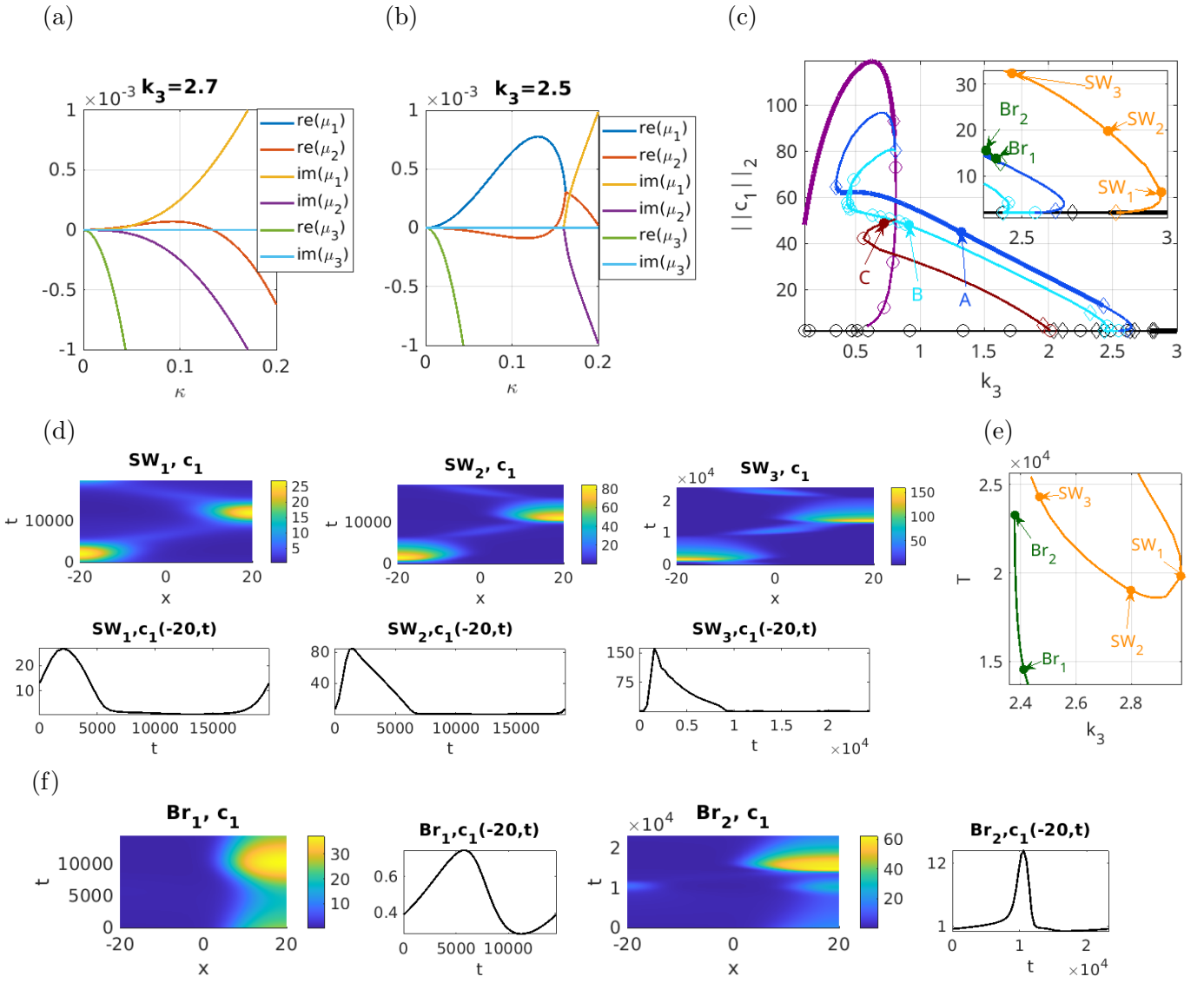

FIGURE 4. Like Fig.3 but with $k_9 = 1$. Loss of stability of $\bar{c}(k_3)$ now via Hopf bifurcations, $\diamond$ symbols. (a) DRs after first two Hopf bifurcations; (b) after first steady bifurcation. (c) BD; the zoom inset also shows the first SW branch (orange), and a breather branch (green). (d) space–time plots (top) of c_1 for the three SWs marked in (c), and behavior of $c_1(t)$ at the left boundary. (e) behavior of period T along Br and SW branches. (f) Samples from the breather branch.

relaxation oscillation behavior as $\|G(t)\|_\infty$ quickly shoots up when a peak develops at either the left or right boundary. In any case, from (a–c) we see that $c(t,\cdot)$ goes back to SW_2, indicating stability of SW_2, although this is just *one* initial perturbation. (d–f) show the results for perturbing SW_3. Here the solution converges to the steady front A (where some influence of damped complex eigenvalues can be seen in the oscillatory behavior of $\|G(t)\|_\infty$ in (e)), yielding instability of SW_3. Additionally we remark that also SW_1 is unstable, as expected from the subcritical bifurcation of the SW branch, as small perturbations yield convergence to $\bar{c}$ here (not shown). Thus, in summary we find that we have a rather small range $k_3 \in (k_{3a}, k_{3b})$ where the SWs are (possibly) stable, $2.47 < k_{3a} < k_{3b} < 3$. The breathers are unstable, as they bifurcate subcritically at the gain of stability of the A branch.

In Fig.6 we consider the "natural parametrization" (NP) setting of (4.8), i.e., again using (4.2) we now combine (4.8) with (4.6) initialized at $k_3 = 5.5$, instead of (4.5) in Fig.3. Thus, while in Fig. 3 $m \in I\!R^3$ changes with k_3 as determined by (2.9b), in Fig.6 all branches (and solutions) shown are at

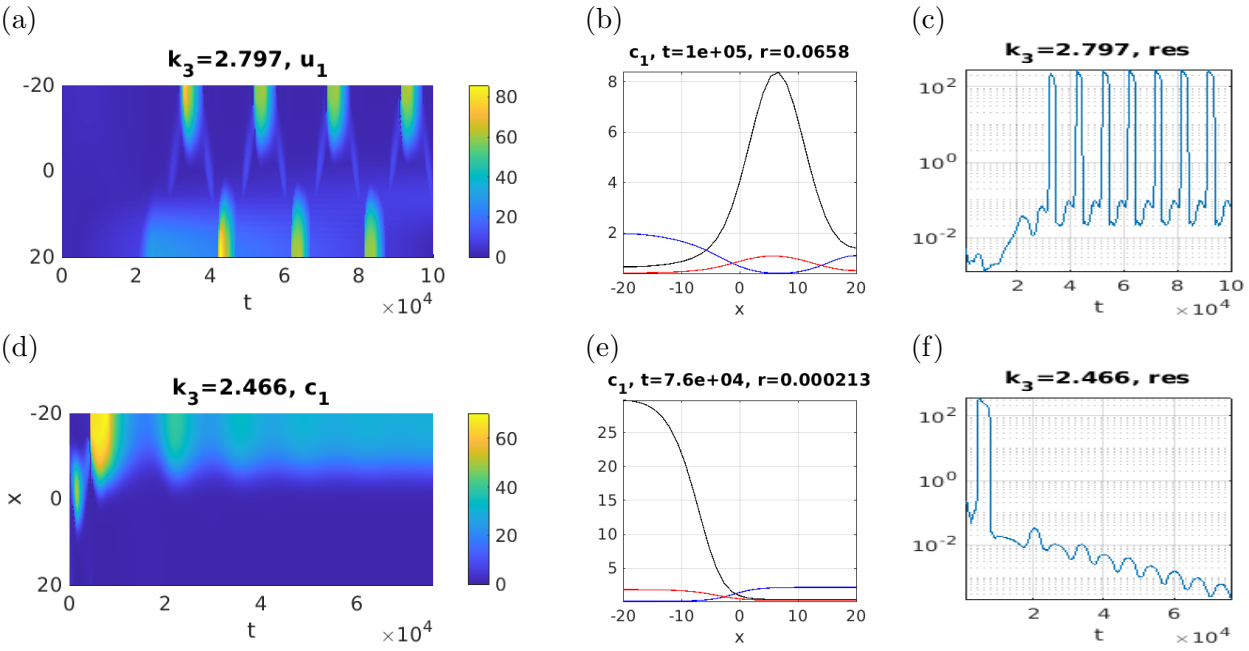

FIGURE 5. DNS for perturbations of SW_2 (a–c) and SW_3 (d–e).

fixed $m \approx (12.4, 25, 640)$. The differences are not significant at large k_3 ($k_3 > 3$, say) but interesting changes happen at smaller k_3:

- The transcritical intersection of $\overline{c}$ and $\widetilde{\overline{c}}$ at $k_3 \approx 0.8$ in Fig.3 now becomes imperfect. That means that the homogeneous branch $\hat{\overline{c}}$ initially approximately follows the $\overline{c}$ branch, but then continuously transitions (as one branch, without bifurcation) to approximately the former $\widetilde{\overline{c}}$ branch. Such breakups of transcritical bifurcations into imperfect bifurcations (separate branches which only "almost intersect") are well known in normal–form theory of bifurcations, see, e.g., [35, §2.5], and the references therein. Note that the black homogeneous branch $\hat{\overline{c}}$ in Fig.8 only shows one half of the recombination under NP of the $\overline{c}$ and $\widetilde{\overline{c}}$ branches from MP.
- At small k_3, the $\hat{\overline{c}}$ branch continues to grow (in $\|c_1\|_2$), while the MP $\widetilde{\overline{c}}$ decreased.

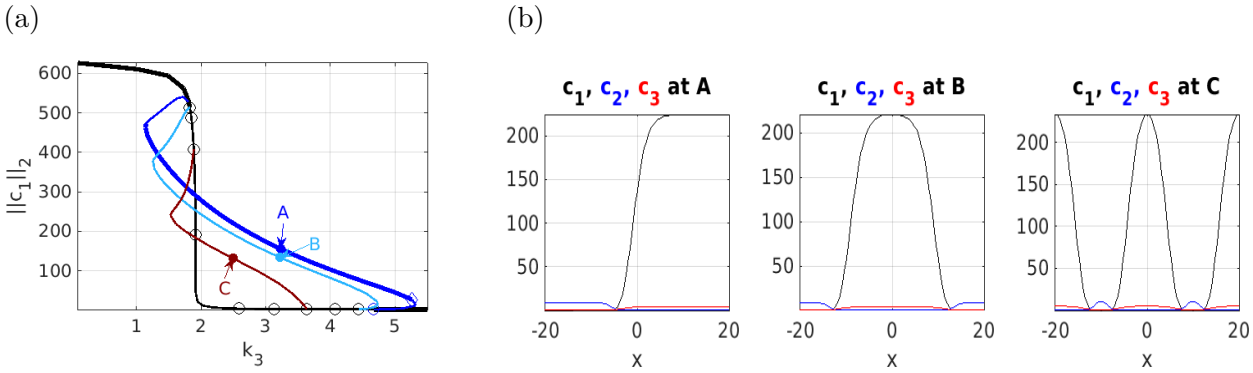

FIGURE 6. The NP setting, $\xi = (2, 1, 1)$ fixed, $k_9 = 0.5$, continuation in k_3, constraints (4.6) with m initialized at $k_3 = 5.5$. Breakup of the $\overline{c}$ — $\widetilde{\overline{c}}$ bifurcation from Fig.3 to an imperfect bifurcation.

Similar transitions to imperfection also occur in other parameter regimes (e.g., $k_9 = 1$ as in Fig.4) when going from MP to NP. However, in summary we find both effects of going from MP to NP *not particularly significant* for the problem from a pattern formation perspective; –they mainly illustrate that the BDs naturally change with the choice of constraints. On the other hand, the occurrence of Hopf bifurcations when going from $k_9 = 0.5$ in Fig.3 to $k_9 = 1$ in Fig.4 and Fig.5 is significant, and in §4.4 we further explore this in 2D.

4.4. **2D.** Fig.7 shows a basic BD for (4.1) on D_R=disk of radius R, here $R = 10$, in the NP setting, using again (4.2) but with (4.3), i.e., $k_9 = 1$, to also discuss Hopf bifurcations again and in particular to compute RWs. The black branch $\bar{c}$ of homogeneous steady states is hence the analog of the black branch from Fig.6, and the primary patterned steady branches belong to Bessel functions v_{mn} with $(m, n) = (1, 1)$ for `A`, $(m, n) = (1, 2)$ for `B`, and $(m, n) = (0, 1)$ for `C` (Mexican hat). In particular, the `A` and `B` branches bifurcate as (subcritical) pitchforks, while the `C` branch bifurcates transcritically. All of these reconnect to $\bar{c}$ at small k_3 and large $\|c_1\|_2$, and $\bar{c}$ regains stability at the reconnection of the `A` branch.

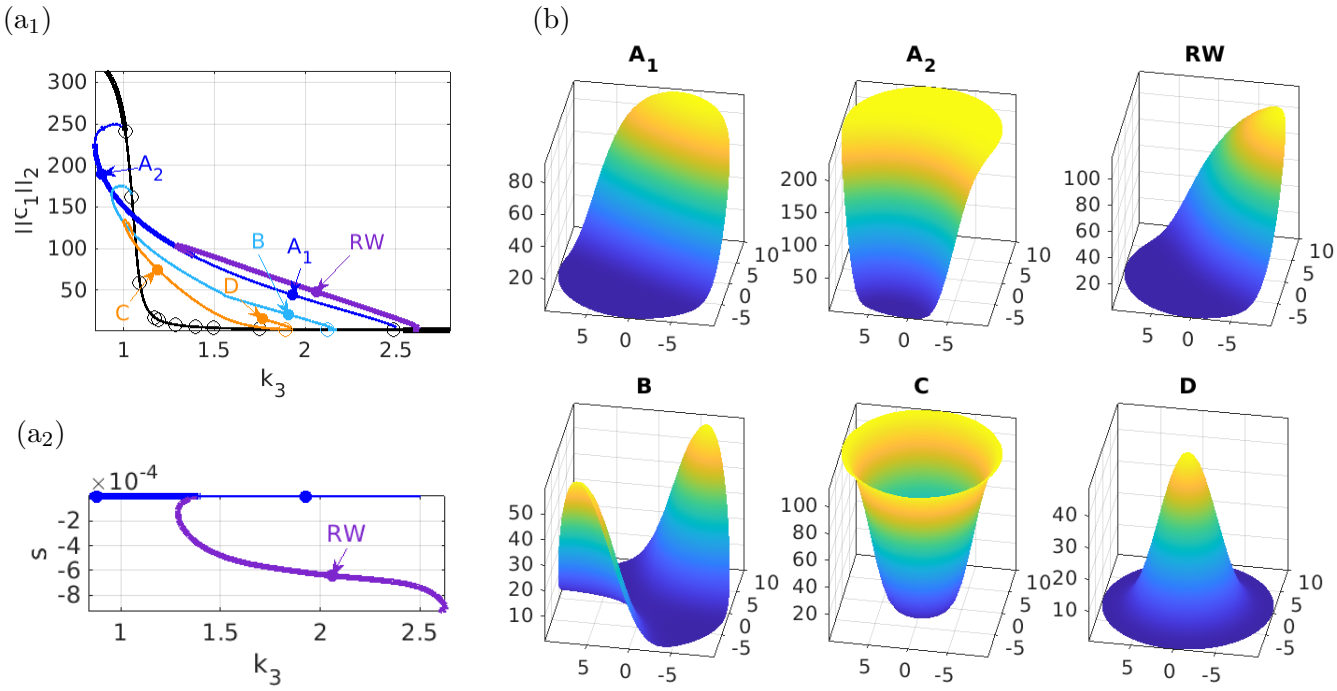

FIGURE 7. (4.1),(4.6) over D_{10}, base parameters (4.2) with $k_9 = 1$. (a) BD of basic steady states (A, dark blue; B, light blue; and C,D, orange), and one RW branch (violet); $\|c_1\|_2$ over k_3 in (a_1) and behavior of speed s along RW branch in (a_2), showing a drift bifurcation of RW from A at $k_3 \approx 1.4$. Samples in (b).

Like in Fig.4, the loss of stability of $\bar{c}$ is due to a Hopf bifurcation with a pair of complex conjugate eigenvalues crossing, with rather small imaginary parts $\mathrm{Im}\mu_{1,2}(k_{3,c}) \approx \pm 0.0008$. By the $O(2)$ equivariance of (4.8) on disks, cf.Remark 4.1b), we then have three bifurcating branches of POs: $\mathrm{RW}_\pm$, and SWs. Since the numerical continuation of SWs is very expensive and since from experience we do not expect SWs to be stable except possibly in narrow parameter regimes (cf.Remark 4.3, and Fig.4), here we focus on RWs, which can cheaply be computed as relative equilibria by going in a co–rotating frame with speed s, cf.(4.8) and the PC (4.9), with initial rotation speed $|s| = |\mathrm{Im}\mu_1(k_{3,c})|$ at bifurcation. Thus continuing in (k_3, s) we obtain Fig.7(a_2) (for a clockwise RW, i.e., negative s), showing that $|s|$ decreases along the `RW` branch, which reconnects to the `A` branch with $s = 0$ around $k_3 = 1.4$. Conversely, the bifurcation of `RW` from `A` is called a *drift bifurcation*, i.e., a steady bifurcation (real eigenvalues crossing the imaginary axis) leading to a (symmetry induced) drifting with speed increasing away from onset.

Importantly, the RWs are linearly (i.e., spectrally) stable between the right and left fold of the RW branch, while the A branch only gains stability at the drift bifurcation of the RWs. This is confirmed by DNS in Fig.8, also illustrating rather large domains of attraction of the respective stable solutions. In (a), with $k_3 = 1.922$, we choose the initial condition $c|_{t=0} = \bar{c}$ with $0.05\cos(2\pi x/10) + C_1$ added to the first component, where C_1 is chosen such that m_3 does not change (and hence all of m, cause m_1, m_2 are not affected anyway). This yields an initial approach to the (unstable) A branch, but

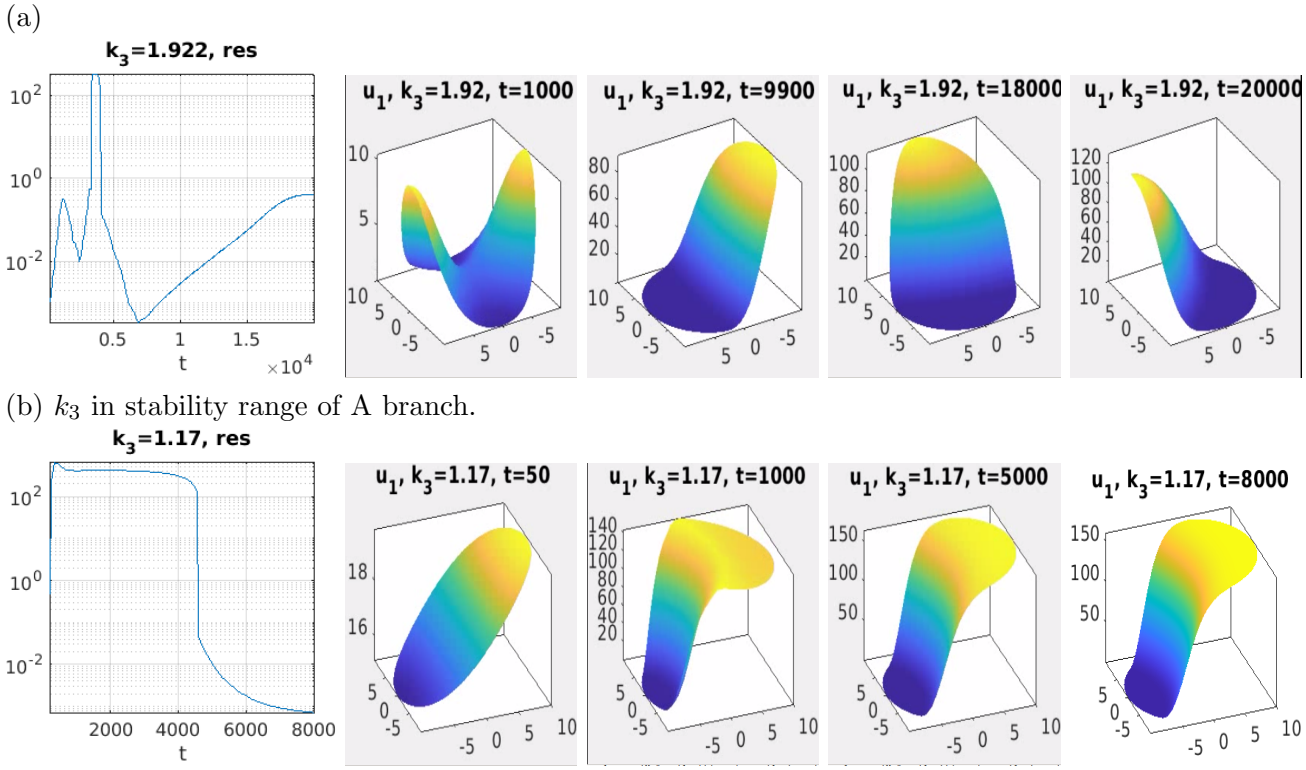

FIGURE 8. DNS for (4.1) over D_{10} with ICs as perturbations of $\bar{c}$ at given k_3. (a) $k \approx 1.1922$; initial approach to A solution, then convergence to RW. (b) $k \approx 1.17$; convergence to A.

then emergence of a rotating waves. This can best be seen by the fact that the residual goes to a nonzero constant. In (b), at $k_1 = 1.17$, we choose $c|_{t=0} = \bar{c}$ with $2\sin(\pi x/20)$ (to shorten transients) added to the first component, and obtain convergence to the A branch.

5. Discussion

Traditionally, deriving instability conditions for networks with a large number of species is mathematically challenging. By restricting our focus to systems that admit a monomial parametrization of their positive steady states, the search for instabilities by analyzing the signs of the leading and constant coefficients of the linearized system's characteristic polynomial becomes feasible. This approach yields sufficient conditions for instability that take the form of simple polynomial inequalities in the reaction rate constants and diffusion coefficients. Furthermore, we translate these algebraic conditions into conditions on the spatial domain size $|\Omega|$ for one-, two-, and three-dimensional spaces.

We apply this framework to a nine-species network modeling the sequential and distributive double (de-)phosphorylation of a protein, and showed that if the catalytic constants and the diffusion coefficients of the enzyme-substrate complexes satisfy condition (1.2), then the homogeneous steady state is destabilized, resulting in the emergence of spatial patterns on appropriately sized domains. This result highlights the practical utility of our method in extracting conditions from complex biochemical models.

To validate and extend these analytical predictions, we perform numerical continuation and direct numerical simulation using the `pde2path` package. The numerical analysis confirms our theoretical predictions. On a 1D domain, the primary loss of stability is confirmed to be of a steady long-wave type, giving rise to subcritical pitchfork bifurcations. However, the numerical exploration also reveals complex dynamics beyond the scope of our determinant-based analysis. By adjusting the rate constant k_9, the primary instability transitions to a Hopf bifurcation. In 1D, this yields time-periodic standing waves and breathers exhibiting relaxation oscillations, while on a 2D disk, it leads to drift bifurcations and the emergence of stable rotating waves.

While our approach provides a starting point for finding sufficient conditions for pattern formation in the system (1.1), it has inherent limitations. The instabilities identified analytically are only Turing-*like*; they represent long-wave (or sideband) instabilities where the first instability is always with respect to nonhomogeneous solutions of the maximal wavelength allowed by the finite domain. The existence of genuine Turing instabilities – characterized by an intrinsic critical wave number independent of the domain size – remains an open problem for this specific PDE system, despite extensive numerical searches across different parameter combinations. Furthermore, because our analytical method relies on the product of eigenvalues, it cannot detect the Hopf bifurcations observed numerically. Thus, while our analytical conditions serve as a guide for identifying steady-state pattern formation, future theoretical work will be required to capture the full spectrum of spatio-temporal dynamics of the system (1.1), including genuine Turing instabilities.

References

1. *Turing patterns, 70 years later*, Nature Computational Science **2** (2022), no. 8, 463–464.
2. Mark S. Ashbaugh and Rafael D. Benguria, *Universal Bounds for the Low Eigenvalues of Neumann Laplacians in N Dimensions*, SIAM Journal on Mathematical Analysis **24** (1993), no. 3, 557–570.
3. C. Conradi, M. Mincheva, and H. Uecker, *Supplementary information;* `Matlab` *sources and documentation*, 2026, Available at [27], tab `Applications`.
4. Carsten Conradi, Elisenda Feliu, and Maya Mincheva, *On the existence of Hopf bifurcations in the sequential and distributive double phosphorylation cycle*, Mathematical Biosciences and Engineering **17** (2020), no. 1, 494–513.
5. Carsten Conradi, Dietrich Flockerzi, and Jörg Raisch, *Multistationarity in the activation of an MAPK: parametrizing the relevant region in parameter space*, Mathematical Biosciences **211** (2008), no. 1, 105–131.
6. Carsten Conradi, Alexandru Iosif, and Thomas Kahle, *Multistationarity in the Space of Total Concentrations for Systems that Admit a Monomial Parametrization*, Bulletin of Mathematical Biology **81** (2019), no. 10, 4174–4209.
7. Carsten Conradi and Maya Mincheva, *Catalytic constants enable the emergence of bistability in dual phosphorylation*, Journal of The Royal Society Interface **11** (2014), no. 95.
8. Carsten Conradi, Maya Mincheva, and Anne Shiu, *Emergence of oscillations in a mixed-mechanism phosphorylation system*, Bulletin of Mathematical Biology **81** (2019), no. 6, 1829–1852.
9. Carsten Conradi and Anne Shiu, *A Global Convergence Result for Processive Multisite Phosphorylation Systems*, Bulletin of Mathematical Biology **77** (2015), no. 1, 126–155 (English).
10. Martin Feinberg, *Foundations of chemical reaction network theory*, Springer.
11. Elisenda Feliu and Nidhi Kaihnsa, *Network reduction and absence of Hopf Bifurcations in dual phosphorylation networks with three Intermediates*, arXiv preprint arXiv:2405.16179 (2024).
12. M. Golubitsky and D. G. Schaeffer, *Singularities and groups in bifurcation theory. Vol. I*, Applied Mathematical Sciences, vol. 51, Springer-Verlag, New York, 1985.
13. M. Golubitsky and I. Stewart, *The symmetry perspective*, Birkhäuser, Basel, 2002.
14. J. Halatek and E. Frey, *Rethinking pattern formation in reaction–diffusion systems*, Nature Physics **14** (2018), 507–514.
15. Katharina Holstein, Dietrich Flockerzi, and Carsten Conradi, *Multistationarity in sequential distributed multisite phosphorylation networks*, Bulletin of Mathematical Biology **75** (2013), no. 11, 2028–2058.
16. R.B. Hoyle, *Pattern formation*, Cambridge University Press., 2006.
17. Jürgen Jost, *Partial differential equations, volume 214 of*, Graduate Texts in Mathematics, Springer, 2013.
18. _____, *Mathematical Methods in Biology and Neurobiology*, Springer, 2014.
19. Krause, Andrew L and Gaffney, Eamonn A and Maini, Philip K and Klika, Václav , *Introduction to 'Recent progress and open frontiers in Turing's theory of morphogenesis'*, Philosophical Transactions of the Royal Society A: Mathematical, Physical and Engineering Sciences **379** (2021), no. 2213, 20200280.
20. J. Krishnan, Lingjun Lu, and Aiman Alam Nazki, *The interplay of spatial organization and biochemistry in building blocks of cellular signalling pathways*, Journal of The Royal Society Interface **17** (2020), no. 166, 20200251.
21. Philip K. Maini and Thomas E. Woolley, *The Turing model for biological pattern formation*, The Dynamics of Biological Systems, Springer, 2019, pp. 189–204.
22. P. C. Matthews and S. M. Cox, *Pattern formation with a conservation law*, Nonlinearity **13** (2000), no. 4, 1293–1320.
23. A. Meiners and H. Uecker, *Helfrich cylinders – instabilities, bifurcation analysis and amplitude equations*, SIADS (2026).
24. Govind Menon and J. Krishnan, *Spatial localisation meets biomolecular networks*, Nature Communications **12** (2021), no. 1, 5357.

25. Mercedes Pérez Millán and Adrián G Turjanski, *MAPK's networks and their capacity for multistationarity due to toric steady states*, Mathematical Biosciences **262** (2015), 125–137.
26. James D. Murray, *Mathematical biology II: spatial models and biomedical applications*, vol. 3, Springer-Verlag, 2001.
27. pde2path, *https://pde2path.uol.de/*, 2026.
28. M. Pérez Millán and A. Dickenstein, *The Structure of MESSI Biological Systems*, SIAM Journal on Applied Dynamical Systems **17** (2018), no. 2, 1650–1682.
29. Mercedes Pérez-Millán, Alicia Dickenstein, Anne Shiu, and Carsten Conradi, *Chemical reaction systems with toric steady states*, Bulletin of Mathematical Biology **74** (2012), 1027–1065 (English).
30. J.D.M. Rademacher and H. Uecker, *Symmetries and freezing of 1D problems in pde2path – a tutorial via some Ginzburg-Landau and FHN models*, 2017, Available at [27].
31. R. Satnoianu, M. Menzinger, and Ph. Maini, *Turing instabilities in general systems*, J. Math. Biol. **41** (2000), no. 6, 493–512.
32. R.A. Satnoianu and P. van den Driessche, *Some remarks on matrix stability with application to Turing instability*, Linear Algebra and its Applications **398** (2005), 69–74, Special Issue on Matrices and Mathematical Biology.
33. Razvan A. Satnoianu, Michael Menzinger, and Philip K. Maini, *Turing instabilities in general systems*, Journal of Mathematical Biology **41** (2000), no. 6, 493–512.
34. Turing, Alan Mathison, *The chemical basis of morphogenesis*, Philosophical Transactions of the Royal Society of London. Series B, Biological Sciences **237** (1952), no. 641, 37–72.
35. H. Uecker, *Numerical continuation and bifurcation in Nonlinear PDEs*, SIAM, Philadelphia, PA, 2021.
36. E. Villar-Sepulveda and A. Champneys, *General conditions for Turing and wave instabilities in RD systems*, Journal of Mathematical Biology **86** (2023), no. 39.
37. Edgardo Villar-Sepúlveda, Alan R. Champneys, and Andrew L. Krause, *Designing reaction-cross-diffusion systems with Turing and wave instabilities*, Journal of Mathematical Biology **91** (2025), no. 4, 37.
38. A. Yochelis, S. Flemming, and C. Beta, *Versatile patterns in the actin cortex of motile cells: Self-organized pulses can coexist with macropinocytic ring-shaped waves*, PRL **129** (2022), 088101.

Hochschule für Technik und Wirtschaft, Berlin, Germany
Email address: carsten.conradi@htw-berlin.de

Department of Mathematical Sciences, Northern Illinois University, DeKalb, IL, USA
Email address: mmincheva@niu.edu

Institut für Mathematik, Carl von Ossietzky Universität Oldenburg, Germany
Email address: hannes.uecker@uni-oldenburg.de